THE ASTROPHYSICAL JOURNAL, 350:700–721, 1990 February 20

A NEW CLASS OF SOLUTIONS FOR INTERSTELLAR MAGNETOHYDRODYNAMIC SHOCK WAVES

W. G. ROBERGE
Department of Physics, Rensselaer Polytechnic Institute
AND
B. T. DRAINE
Princeton University Observatory
Received 1989 May 15; accepted 1989 August 23

ABSTRACT

An analysis is presented of the equations of motion for steady magnetohydrodynamic (MHD) shock waves propagating in interstellar clouds, for boundary conditions that preclude C shocks. In addition to J shocks, in which the neutral fluid component becomes subsonic at an adiabatic jump front, the equations admit a new class of solutions, called C* shocks, in which the transition to subsonic flow occurs continuously at a sonic point. Numerical methods are developed for computing the structure of J and C* shocks propagating in diffuse interstellar clouds; the effects of chemical, ionization, and recombination processes are included in this treatment. An alternative numerical method, which uses "artificial viscosity" to facilitate integration through sonic points, is analyzed and shown to be invalid. A set of exemplary solutions, computed for realistic shock parameters, shows that C* shocks occur for a broad range of conditions relevant to diffuse interstellar clouds.

Subject headings: hydromagnetics — interstellar: matter — shock waves

I. INTRODUCTION

Shock waves are ubiquitous in the interstellar medium. They are driven by supernova explosions, stellar and protostellar winds, expansion of photoionized gas, and cloud-cloud collisions (McCray and Snow 1979). The frequency of occurrence of shock waves in diffuse interstellar clouds may be estimated theoretically (e.g., Draine and Salpeter 1979), but it can also be determined empirically from the overall abundance of CH^+, because CH^+ seems to be formed primarily in shock-heated gas. The result is that perhaps one in three diffuse clouds contains, at a given moment, a shock with speed $v_s > 5$ km s^{-1} (Draine and Katz 1986*b*).

Because of the presence of interstellar magnetic fields, a multifluid MHD treatment is often required to describe shocks in media, such as interstellar clouds, where the fractional ionization is low (Mullan 1971; Draine 1980, hereafter D80; Chernoff 1987, hereafter C87). In this multifluid picture, there are two distinct speeds at which compressive disturbances may be communicated. In the *charged* component of the plasma, disturbances propagating perpendicular to the magnetic field $\boldsymbol{B}$ travel at the ion magnetosonic speed,

$$c_{\rm ims} \simeq 218\left[\frac{(B/\mu{\rm G})^2}{(x/10^{-4})(n/{\rm cm}^{-3})(\mu_i/m_p)}\right]^{1/2} {\rm km\ s}^{-1}\,, \tag{1.1}$$

where x, n, and μ_i are, respectively, the fractional ionization, total (charged plus neutral) number density of the gas, and ion mean molecular weight. Compressive disturbances in the *neutral* gas travel at the neutral sound speed, given by

$$c_n = 0.29\left[\frac{\gamma(T_n/10\ {\rm K})}{(\mu_n/m_p)}\right]^{1/2} {\rm km\ s}^{-1}\,, \tag{1.2}$$

in terms of the temperature, T_n, mean molecular weight, μ_n, and adiabatic exponent, γ, of the neutral component. In shocks with speeds v_s in the range $c_n \lesssim v_s \lesssim c_{\rm ims}$, the charged fluid is accelerated upstream from the neutrals, and ion-neutral streaming motions occur throughout a "magnetic precursor" (Mullan 1971; D80).

The structure of shocks with magnetic precursors depends on the ratio of the cooling time, τ_c, in the neutral gas, to the time scale τ_a for the neutrals to be accelerated by streaming ions. If $\tau_c \gg \tau_a$, then the acceleration process is effectively adiabatic, the Rankine-Hugoniot jump conditions (Landau and Lifshitz 1959) uniquely relate the hydrodynamical variables on either side of the magnetic precursor, and a "single-fluid" description may be used to describe the subsequent evolution of the shock. This single-fluid picture is valid at low magnetic field strengths or large fractional ionizations (where the width of the magnetic precursor becomes small; see D80) and large shock speeds (where the amount of thermal energy to be dissipated becomes large and ionizing radiation produced inside the shock may increase the preshock fractional ionization; see Shull and McKee 1979; Hollenbach and McKee 1979). For typical physical conditions inside interstellar clouds, the single-fluid picture applies to shocks with speeds greater than 40–50 km s^{-1} (Hollenbach, Chernoff, and McKee 1989).

In the opposite limit, where $\tau_c \ll \tau_a$, the accelerating neutral fluid remains cool enough to be supersonic everywhere (in the reference frame where the shock is stationary). In this case, all the hydrodynamical variables are continuous, and the shock is termed "C-type" (D80). Because they contain no sonic points, C shocks may be computed straightforwardly by using initial value methods. C-type shock models have been proposed to explain the intense molecular line emission from OMC-1 (Draine and

Roberge 1982; Chernoff, Hollenbach, and McKee 1982), and to account for the abundance of CH^+ toward ζ Oph and other well-studied stars (Draine and Katz 1986*b*; Draine 1986*b*; Pineau des Forêts *et al.* 1986). Most studies of C shocks have assumed them to be "steady" (i.e., time independent) and "perpendicular" (with θ, the angle between the preshock magnetic field and the direction of shock propagation, equal to 90°). "Oblique" C shocks, with arbitrary θ, have been studied by Wardle and Draine (1987) and were found to be qualitatively similar to "perpendicular" C shocks, provided θ is not too small. The possibility of nonsteady C shocks has been examined recently by Wardle (1990), who found that C shocks are stable provided that the Alfvén Mach number $M_a \lesssim 5$, but instabilities involving "buckling" of the magnetic field lines may grow for $M_a \lesssim 5$.

This paper considers shock waves that fall between the limiting cases of single-fluid and C-type shocks, where radiative cooling in the magnetic precursor is nonnegligible but is nevertheless insufficient to keep the neutral gas supersonic throughout the flow. In some cases, the transition to subsonic flow takes place at a thin "jump front," i.e., a region where molecular viscosity effects the transition adiabatically, over a few collision mean free paths. The onset of so-called J shocks typically occurs when the shock speed exceeds a critical value which depends on the preshock magnetic field strength and other preshock conditions; the transition from C- to J-type solutions has been discussed by Chernoff, Hollenbach, and McKee (1982), and more recently by Hollenbach, Chernoff, and McKee (1989). Because the magnetic precursor is nonadiabatic, the hydrodynamical variables at the jump front, which are required to implement the Rankine-Hugoniot relations, are not known *a priori*. As described below, finding the variables at the jump front is a two-point boundary value problem, so that methods employed for computing C shocks are inapplicable. Draine (D80) computed a few illustrative J-type solutions using a finite difference technique, but stiffness of the fluid equations makes this approach very computationally intensive. Mullan (1971) and Chernoff (C87) discussed efficient methods for calculating J shocks when one knows the downstream boundary conditions for the flow *a priori*. However, this approach cannot be extended readily to include the effects of shock chemistry. Flower and Pineau des Forêts (1987, hereafter FPdF87) have presented a method for computing J shocks, using modified equations of motion for the fluids. Unfortunately, however, their method is invalid for several reasons, as described in Appendix A.

In the following sections, we develop iterative methods for computing the structure of transonic, MHD shocks in diffuse interstellar clouds. The present study will be restricted to shocks that are both steady and "perpendicular." The relevant equations and boundary conditions are summarized in § II. In the course of this work, a new class of hydrodynamical solutions was discovered in which the compression ratio across the jump front goes to unity for a broad range of realistic shock parameters. Chernoff, to whom we communicated this discovery in advance of publication, also found the new solutions in an analytical study of shocks with power-law cooling functions and termed them "C* shocks" (C87). Because the existence of C* shocks is surprising, we use the analytical methods developed by Chernoff (C87) in § III to show why C* solutions are expected for a nonnegligible set of shock parameters. Numerical methods suitable for computing J and C* shocks in diffuse clouds are described in § IV. (Readers who are not interested in the methods per se may wish to skip this section.) In § V, the methods are applied to calculate some exemplary solutions for realistic shock parameters. In § VI, we give a physical explanation for an empirical result described in § V, that C* shocks are the predominant solution form for intermediate shock speeds ($18 \lesssim v_s \lesssim 30$ km s^{-1}) in diffuse clouds. Our results are summarized in § VII.

II. MAGNETOHYDRODYNAMICS

The MHD equations describing a partially ionized, chemically reacting fluid have been derived elsewhere (Draine 1986*a*). For plane-parallel, steady flows, with the preshock magnetic field assumed to be perpendicular to the direction of shock propagation, these equations reduce to a set of coupled, nonlinear, ordinary differential equations, in which the independent variable is spatial position, z, measured in a reference frame comoving with the shock. When solved for derivatives of the dependent variables, the latter reduce to

$$\frac{dv_n}{dz} = \frac{2/3[G_n - N_n u_n - (\rho_n v_n/\mu_n)(du_n/dz)] - F_n v_n + S_n v_n^2}{\rho_n(c_n^2 - v_n^2)}, \tag{2.1}$$

$$\frac{dv_i}{dz} = \frac{2/3(G_i + G_e) + F_n v_i - S_n v_i^2}{\rho_i[(B_0^2/4\pi\rho_i)(v_s^2/v_i^2) + 5/3(kT_s/\mu_i) - v_i^2]}, \tag{2.2}$$

$$\frac{dT_n}{dz} = \frac{\mu_n}{\rho_n v_n k}\left[F_n v_n - S_n v_n^2 - N_n k T_n + \left(\frac{\rho_n k T_n}{\mu_n} - \rho_n v_n^2\right)\frac{dv_n}{dz}\right], \tag{2.3}$$

$$\frac{dT_s}{dz} = \frac{\mu_i}{\rho_i v_i k}\left\{-F_n v_i + S_n v_i^2 - N_i k T_s + \left[\frac{\rho_i k T_s}{\mu_i} + \frac{B_0^2}{4\pi}\left(\frac{v_s^2}{v_i^2}\right) - \rho_i v_i^2\right]\frac{dv_i}{dz}\right\}, \tag{2.4}$$

and

$$\frac{dT_d}{dz} = \frac{\mu_i}{\rho_i v_i k}\left[\frac{2}{3}(G_i - G_e) - N_i k T_d\right] - \frac{2}{3}\frac{T_d}{v_i}\frac{dv_i}{dz}. \tag{2.5}$$

The subscripts "n", "i", and "e" above refer, respectively, to quantities in the neutral, ion, and electron fluids. The mass density, mean molecular weight, mean internal energy per particle, bulk velocity, and kinetic temperature of fluid f are denoted by ρ_f, μ_f, u_f, v_f, and T_f, respectively. The dependent variables in equations (2.4) and (2.5) are $T_s \equiv T_i + T_e$ and $T_d \equiv T_i - T_e$. The quantity B_0 is the preshock magnetic field strength, v_s is the shock speed, and $c_n \equiv (5kT_n/3\mu_n)^{1/2}$ is the adiabatic sound speed in the neutral fluid. The preceding equations incorporate the assumption that the magnetic field is frozen into the ion/electron fluid, so that $B(z) = B_0 v_s/v_i$,

and that the ions are structureless particles, so that $u_i = 0$. The source terms N_f and S_f, which would vanish in the absence of ionization, recombination, or other chemical processes, are the net rates per unit volume at which particles and mass, respectively, are added to fluid f. The source term F_n is the rate per unit volume at which the momentum of the neutral fluid is changed, as a result of ion-neutral scattering, ionization, or recombination. The source term G_f is the rate per unit volume at which thermal energy is added to fluid f by ion-neutral scattering, photoelectric heating, photodissociation, radiative cooling, etc. (see Draine 1986*a*).

To close equations (2.1)–(2.5), values are required for the spatially dependent quantities μ_n, ρ_n, μ_i, and ρ_i. This paper considers shocks with speeds sufficiently small so that collisional and radiative ionization of hydrogen and helium within the shock are negligible. Thus, one may write $\rho_n v_n = \rho_{n0} v_s$ (the subscript "0" refers to the preshock value of a quantity) and neglect the small effect on ρ_n due to possible recombination of the metals. The quantities μ_n, ρ_i, and μ_i are derived from the number densities of various chemical species in the ion and neutral fluids. Thus, in addition to equations (2.1)–(2.5), a reaction network of the form

$$\frac{d}{dz}(n_j v_j) = C_j , \qquad j = 1, \ldots N_c , \tag{2.6}$$

is solved, where n_j, v_j, and C_j are the number density, bulk velocity, and net rate of creation per unit volume, respectively, of the jth chemical species in the network. Chemical reactions in the flow have been computed following Draine and Katz (1986*a*), except that (1) the products of CH^+ photodissociation are now assumed to be C and H^+ (rather than C^+ and H), and (2) the reaction network has been extended to $N_c = 32$ species by including simple sulfur chemistry. These changes will be described fully in a future paper, in which chemistry in the types of shocks considered here will be examined in greater detail.

The extact upstream boundary conditions, that the fluid should be undisturbed, apply only infinitely far upstream. The solutions in this paper therefore satisfy approximate boundary conditions, in which the shock begins at a fiducial point, $z = 0$, where the shock has perturbed the neutral velocity by $\delta v_n = -10^{-4} v_s$. Perturbations in the other hydrodynamical variables are computed in terms of δv_n and the unperturbed variables by linearizing equations (2.1)–(2.5) about the unperturbed state (see D80). For particular choices of the parameters that specify preshock conditions (see Table 1), the upstream variables T_{n0}, T_{i0}, T_{e0} and n_{j0} are found numerically, by requiring each of the fluids to be in thermal balance and the chemistry to be in a steady state. We neglect perturbations in the chemical abundances; i.e., we begin the integration with the equilibrium values of n_j/n_H. This is an excellent approximation for two reasons. First, linearization of the equations upstream reveals only one exponentially growing mode. Therefore, if we start with an arbitrary *small* perturbation to the initial conditions (e.g., suppose we perturb only v_i), after we have integrated numerically a distance downstream corresponding to a few exponentiation lengths, we will have a solution which is in practice indistinguishable from what we would have obtained from full linearization of the equations. Second, all species of interest either as thermally-important coolants (e.g., H_2 or C^+), or as dynamically-important neutrals (H or H_2), or ions (H^+ or C^+) respond very slowly to small changes in the physical conditions. For example, for the initial conditions in Table 1, the "chemical time scale" for H_2 is of order 10^{14} s, because both photodissociation of H_2 and formation of H_2 on grains are slow processes. These chemical time scales are orders of magnitude larger than the time scale on which the hydrodynamical perturbations grow. (In the numerical models discussed in § V, the latter time scale varies from 10^8 s to a few times 10^{10} s). Neglecting the chemical perturbations at the starting point of the integration therefore has a negligible effect on the overall shock.

The downstream boundary conditions are, likewise, that the medium should be in thermal and chemical balance. In practice, however, it is impossible to implement these conditions: In shocks with chemistry, the downstream values of n_j are not known *a priori* and, in any case, the equilibrium values apply only at $z = \infty$. This is one of the arguments in favor of the approach adopted in this paper. Briefly, the shock structure is calculated by computing a series of solutions, in each case integrating equations (2.1)–(2.6) forward in z from the initial, perturbed state. Solutions computed in this way will, in some cases, diverge from the desired final state as z increases. In such cases, the divergent solutions are periodically "refined" during the forward integration, using shooting methods described in § IV. The model terminates when the convergent solution has propagated far enough to satisfy a predefined

TABLE 1

PRESHOCK CONDITIONS

Quantity	Value	Notes
n_H^0	25 cm^{-3}	Density of H nuclei
B_0	5 μG	Magnetic field, assumed $\perp v_s$
ζ_{cr}	10^{-17} s^{-1}	Primary cosmic ray ionization rate of H
ζ_{H_2}	2×10^{-14} s^{-1}	H_2 photodestruction rate
χ_{uv}	1	Diffuse UV intensity relative to Draine 1978
H_2 o/p	3	H_2 ortho/para ratio
A_C	2×10^{-4}	Carbon abundance (relative to H)
A_O	7×10^{-4}	Oxygen abundance (relative to H)
T_{n0}	42 K	Neutral temperature
T_{i0}	58 K	Ion temperature
T_{e0}	58 K	Electron temperature
n(H)	23 cm^{-3}	Density of H atoms
$n(H_2)$	0.87 cm^{-3}	Density of H_2
$x(e)$	4.0×10^{-4}	n_e/n_H
$x(C^+)$	2.0×10^{-4}	$n(C^+)/n_H$
$x(H^+)$	1.5×10^{-4}	$n(H^+)/n_H$
$x(S^+)$	2.0×10^{-5}	$n(S^+)/n_H$
x(metals)	2.0×10^{-5}	n/n_H for ionized metals, excluding C^+ and S^+

criterion, typically that the neutral temperature has dropped below some fiducial value. This generally ensures that the variables are close to their equilibrium values.

III. PHASE PORTRAIT ANALYSIS

a) *Chernoff's Phase Space Description*

As shown by Chernoff (C87), it is instructive to visualize shock solutions as trajectories in the phase space of solution variables, where the spatial coordinate z plays the role of time. The utility of this approach follows from two approximations introduced by Chernoff, which are valid when the fractional ionization is sufficiently small and which effectively reduce the phase space to two dimensions. Specifically, one neglects thermal and ram pressure of the ion/electron fluid compared to $B^2/8\pi$ and treats the charged fluid as being in a state of thermal balance (i.e., one sets $G_i + G_e = 0$; see C87 for details.) If one assumes further that the internal energy density u_n is proportional to the neutral temperature, then u_n may be replaced by $([5 - 3\gamma]/2[\gamma - 1])kT_n$. With these assumptions, the equations for conservation of neutral momentum, ion + electron momentum, and neutral energy simplify to

$$\frac{d}{dz'}\left(r + \frac{t}{r}\right) = \frac{(q - r)}{r}, \tag{3.1}$$

$$\frac{d}{dz'}\left(\frac{1}{2} M_{nA}^{-2} q^{-2}\right) = \frac{-(q - r)}{r}, \tag{3.2}$$

and

$$\frac{d}{dz'}\left(\frac{1}{2} r^2 + \frac{\gamma}{\gamma - 1} t\right) = q\,\frac{(q - r)}{r} + H_n, \tag{3.3}$$

in terms of the dimensionless variables $r \equiv v_n/v_s$, $q \equiv v_i/v_s$, $t \equiv kT_n/\mu_n v_s^2$, the neutral Alfvén Mach number $M_{nA} \equiv v_s/(B_0^2/4\pi\rho_{n0})^{1/2}$, the adiabatic index γ ($= 5/3$ for a monatomic gas), and the dimensionless distance z', defined by

$$\frac{dz'}{dz} \equiv \frac{\mu_i n_e \langle\sigma v\rangle_{in}}{(\mu_n + \mu_i) v_s}. \tag{3.4}$$

In equation (3.4), $\langle\sigma v\rangle_{in}$ is the momentum transfer rate coefficient for elastic ion-neutral scattering, and H_n is the net rate (in units of $\rho_{n0} v_s^3 [dz'/dz]$) at which thermal energy is added to the neutrals, due to all heating and cooling processes *except* elastic ion-neutral scattering. In Chernoff's notation, $H_n = -\Psi t/r$.

The system of equations (3.1)–(3.3) admits the integral (C87)

$$t(q, r) = r[1 - r + \tfrac{1}{2} M_{nA}^{-2}(1 - q^{-2})] \tag{3.5}$$

(where it has been assumed that the flow is cold initially, i.e. $t = 0$ at $z = -\infty$). This leaves two independent equations,

$$\dot{q} = M_{nA}^2 q^3 \frac{(q - r)}{r}, \tag{3.6}$$

and

$$\dot{r} = \frac{(\gamma - 1)\{(r - q)[\gamma r/(\gamma - 1) - q] + H_n r\}}{\gamma t - r^2}, \tag{3.7}$$

where the dot denotes differentiation with respect to z'. These equations can be cast in the autonomous form

$$\frac{dr}{dq} = \frac{R(q, r)}{Q(q, r)} \tag{3.8a}$$

$$R(q, r) \equiv (\gamma - 1)\left[(r - q)\left(\frac{\gamma}{\gamma - 1} r - q\right) + H_n r\right] \tag{3.8b}$$

$$Q(q, r) \equiv M_{nA}^2 q^3 r^{-1}(r^2 - \gamma t)(r - q). \tag{3.8c}$$

In the units employed here, the adiabatic sound speed of the neutral fluid is $(\gamma t)^{1/2}$, so that Q is proportional to $(v_n^2 - c_n^2)$.

The trajectories $r(q)$ satisfying equation (3.8) are an exact description of the hydrodynamics granted the two assumptions outlined above. The hydrodynamics can therefore be computed from equation (3.8) alone, if one assumes that H_n is a known function of q and r. The analysis in § III adopts this assumption, which amounts to neglecting the effects of chemistry on the cooling rate of the neutral gas. This is a good approximation for nondissociative shocks in diffuse clouds, where the cooling is dominated by H_2 and C^+ with nearly constant abundances. Consequently, the results of the analysis in § III are used to formulate numerical methods for diffuse cloud shocks including chemistry. The validity of this approach is examined in § IV, which discusses the errors which might be introduced as a result of coupling between cooling and chemistry.

Figure 1 is a picture of the phase space, showing certain curves defined by Chernoff. The equilibrium states U, upstream, and D, downstream from the shock lie on the intersection of the curves $q = r$, on which compression of the ion-electron fluid by drag forces vanishes, and $R = 0$, on which compression of the neutrals by drag plus neutral pressure gradients vanishes. The neutral flow is

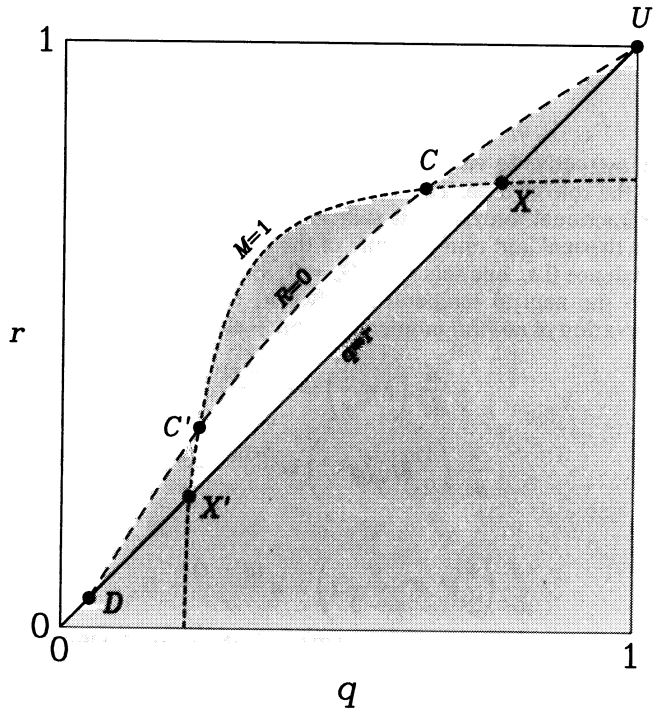

FIG. 1.—(After Chernoff 1987, Fig. 6). The two-dimensional phase space in which solutions to eq. (3.8) are defined. Variables q and r are the dimensionless ion and neutral velocities, respectively. Points U and D are the upstream and downstream equilibrium states. Physical solutions are excluded from the shaded regions because trajectories passing through such regions cannot satisfy the boundary conditions at U and D. The neutral fluid is supersonic above the $M = 1$ line and subsonic below it. On $R = 0$, expression (3.8b) vanishes, and dr/dq is zero. The sonic points, C and C′, are the only places where a supersonic trajectory may pass into the subsonic region continuously, i.e., without passing through an adiabatic "jump" in the neutral fluid variables (via a "viscous subshock").

supersonic above and subsonic below the curve $M = 1$, on which the neutral Mach number $M = r/(\gamma t)^{1/2}$ is unity, the function Q vanishes, and $dr/dq = \pm\infty$. Sonic points are possible only where $R = 0$ intersects $M = 1$; in this paper, we will assume that the downstream point D has $M > 1$, in which case there must be an even number of sonic points. (It should be mentioned that all our results, including numerical methods, are applicable to cases where the downstream sonic point D has $M < 1$ and the number of sonic points is odd.)

In most cases, we will assume that exactly two sonic points, labeled C and C′, exist as shown in Figure 1, although in § III*d* below we will discuss the occurrence of more than two sonic points. In Figure 1, only the unshaded regions of phase space are physically relevant. The shaded regions are excluded, either because trajectories beginning at U cannot enter them or because trajectories entering them cannot reach *D* (i.e., satisfy the downstream boundary conditions).

A continuous trajectory which satisfies equation (3.8) at all points is a member of the class of C or C* shocks. Trajectories containing "discontinuities" are also of physical interest, provided that the flow variables satisfy the Rankine-Hugoniot relations (e.g., Landau and Lifshitz 1959) across the discontinuity. For the flows considered here, the ion-electron fluid is always sub-magnetosonic, and therefore $q = v_i/v_s$ varies continuously. If, however, the neutral fluid is supersonic, mass, momentum, and energy can be conserved in a discontinuous "jump" in the neutral flow variables satisfying the jump conditions

$$r_2 = r_1\left[\frac{\gamma - 1}{\gamma + 1} + \frac{2\gamma}{\gamma + 1}\frac{t_1}{r_1^2}\right], \tag{3.9}$$

$$t_2 = t_1 + \frac{\gamma - 1}{2\gamma}(r_1^2 - r_2^2)\,. \tag{3.10}$$

In the phase space of Figure 1, such a "jump" appears as a vertical drop from a point (q, r_1) above the $M = 1$ curve to a point (q, r_2) below the $M = 1$ curve. The "jump" actually occurs over a distance of order the molecular mean free path, and it is brought about by viscous stresses and viscous dissipation within this narrow transition zone. Such a "jump" in the neutral fluid variables will therefore be referred to as a "viscous subshock."

b) Local Analysis of Flow Near Sonic Points

Consider a sonic point (q_c, r_c) where, by definition, $Q = R = 0$. The right-hand side of equation (3.8a) is formally indeterminate at such points. To see this, let (ρ, θ) be the polar coordinates of an arbitrary point (q, r),

$$q = q_c + \rho\cos\theta\,, \tag{3.11a}$$

$$r = r_c + \rho\sin\theta\,, \tag{3.11b}$$

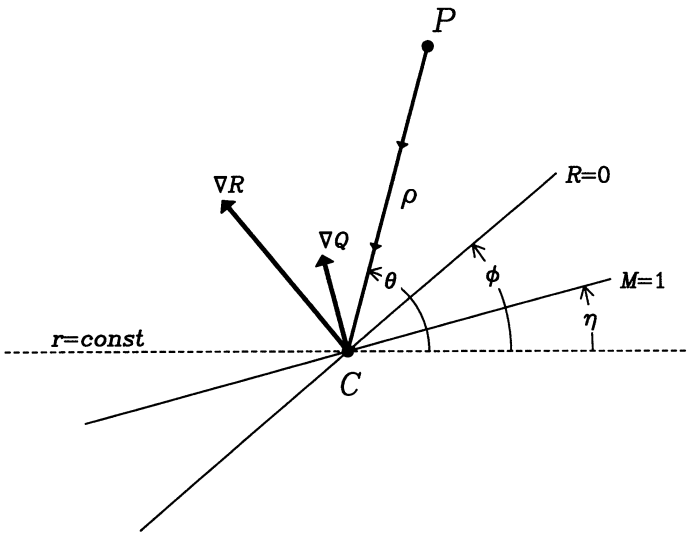

FIG. 2.—Definition of quantities used to evaluate the limit in eq. (3.12). The angles η and ϕ, respectively, orient the lines $M = 1$ and $R = 0$ in the phase plane. Their intersection is a sonic point, which in practice may be either point C (if $\phi > \eta$) or C′ (if $\phi < \eta$). The limit is taken as the point P approaches C, along a ray oriented at angle θ.

and consider the limit of R/Q as θ stays fixed and $\rho \to 0$ (see Fig. 2). Expanding Q and R to first order in ρ, one finds

$$\frac{dr}{dq} = \lim_{\rho \to 0} \frac{|\nabla R|\ \rho \sin(\theta - \phi) + O(\rho^2)}{|\nabla Q|\ \rho \sin(\theta - \eta) + O(\rho^2)} = \alpha \frac{\sin(\theta - \phi)}{\sin(\theta - \eta)} + O(\rho)\,, \tag{3.12}$$

$$\alpha \equiv \frac{|\nabla R|}{|\nabla Q|}\,, \tag{3.13}$$

where $|\boldsymbol{x}|$ denotes the norm of vector $\boldsymbol{x}$, and the two angles ϕ and η, defined in Figure 2, specify the orientation in the phase plane of the curves $R = 0$ and $M = 1$, respectively. Equation (3.12) shows that dr/dq is not uniquely defined at a sonic point, because the limit above depends on the direction θ from which a trajectory approaches. A corollary is that ray PC in Figure 2 is generally not a trajectory of the equation of motion, equation (3.8), because the "velocity vector" $\dot{q}(1, dr/dq)$ will not be tangent to PC if θ is chosen arbitrarily. Outside the sonic point, the trajectories within an infinitesimal neighborhood obey

$$\frac{dr}{dq} = \alpha \frac{\sin(\theta - \phi)}{\sin(\theta - \eta)}\,. \tag{3.14}$$

The solutions of equation (3.14) are analyzed in Appendix B, with the following results.

i) *The Upstream Sonic Point*, C

There are only three generic possibilities for the flow, depending on the value of α relative to

$$\alpha^{\pm}_{\rm crit} = \frac{\sin\phi\cos\eta + \sin(\phi - \eta) \pm 2[\sin\phi\cos\eta\sin(\phi - \eta)]^{1/2}}{\cos^2\phi}\,. \tag{3.15}$$

If $\alpha > \alpha^{+}_{\rm crit}$ or $\alpha < \alpha^{-}_{\rm crit}$, then the flow contains two special trajectories, called $\hat{\theta}_1$ and $\hat{\theta}_2$, which are straight lines that pass continuously through the sonic point. The angles $\hat{\theta}_1$ and $\hat{\theta}_2 > \hat{\theta}_1$ that are used to label these lines are given explicitly by

$$\tan\hat{\theta}_{1,2} = \frac{\sin\eta + \alpha\cos\phi \mp W^{1/2}}{2\cos\eta}\,, \tag{3.16a}$$

$$W \equiv \alpha^2\cos^2\phi + 2\alpha(\sin\eta\cos\phi - 2\sin\phi\cos\eta) + \sin^2\eta\,. \tag{3.16b}$$

Phase portraits for the generic flow fields are given in Figure 3, for the cases where $\alpha < \alpha^{-}_{\rm crit}$ (Fig. 3*a*), $\alpha^{-}_{\rm crit} < \alpha < \alpha^{+}_{\rm crit}$ (Fig. 3*b*), and $\alpha > \alpha^{+}_{\rm crit}$ (Fig. 3*c*). The first two cases do not admit continuous transonic flow from the supersonic to the subsonic region. Thus, if $\alpha < \alpha^{+}_{\rm crit}$ then the *solution trajectory* which satisfies the boundary conditions at U and D must be either a C shock (i.e., everywhere supersonic) or a J shock (discontinuous jump from supersonic to subsonic flow). One cannot distinguish betwen these possibilities on the basis of a local analysis alone, because the boundary conditions satisfied by the trajectories in Figures 3*a* and 3*b* are unknown.

If $\alpha > \alpha^{+}_{\rm crit}$, however, continuous super- to subsonic flow may occur. As shown in Appendix B, $\hat{\theta}_1$ attracts trajectories and $\hat{\theta}_2$ repels them in the supersonic region. Thus $\hat{\theta}_1$ and $\hat{\theta}_2$ separate the supersonic flow into three nonintersecting regions. Trajectories with $\theta < \hat{\theta}_1$, which are emitted by $M = 1$, are unphysical because they fail to satisfy the boundary conditions at U. Trajectories with $\theta > \hat{\theta}_2$ are absorbed by $M = 1$. The solution trajectory may consist in part of a trajectory of this type, if the latter is connected by a

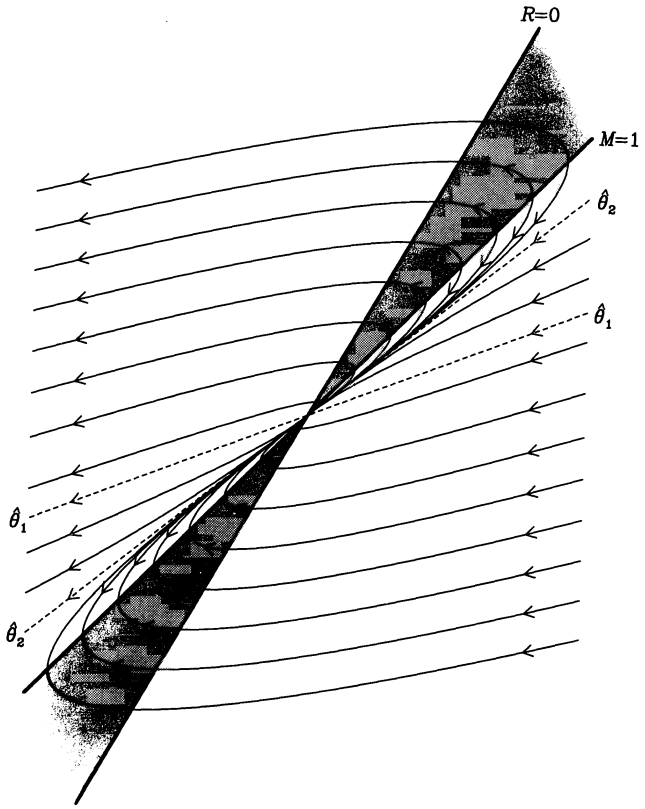

FIG. 3*a*

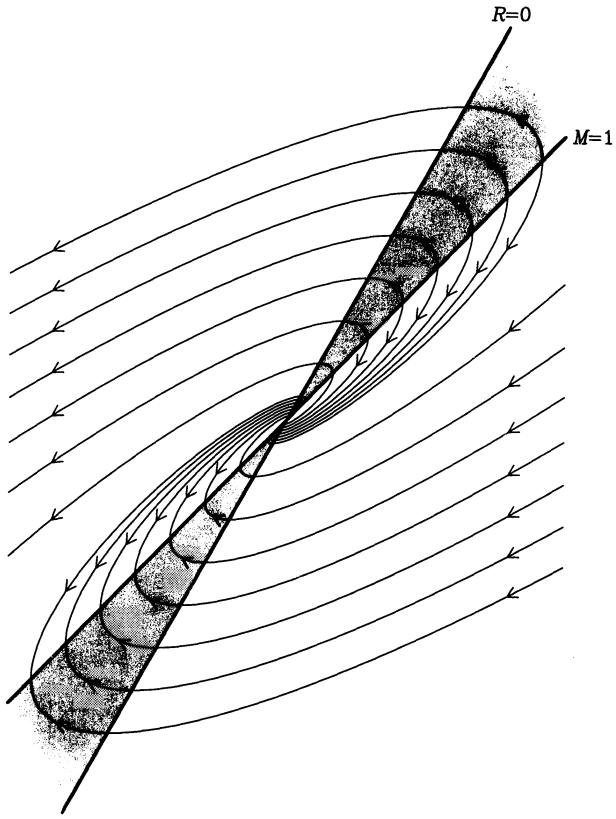

FIG. 3*b*

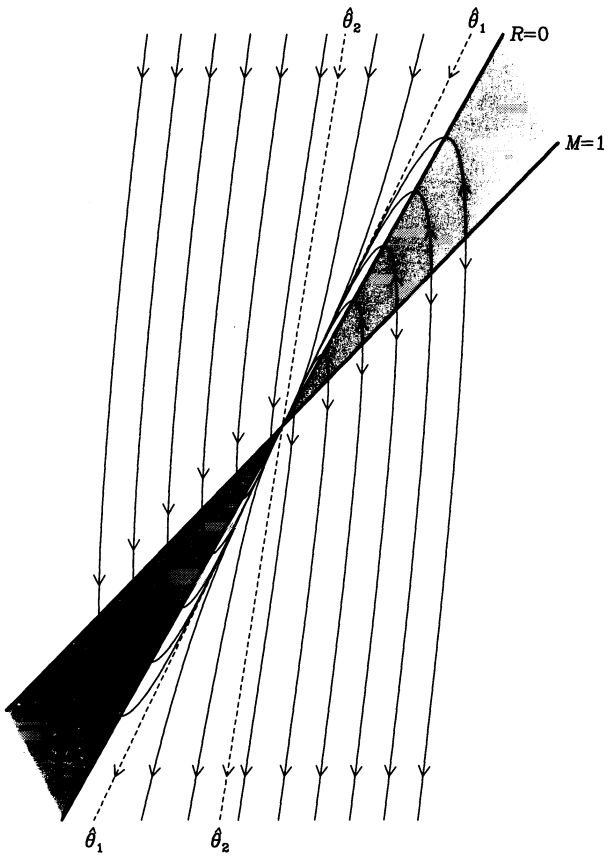

FIG. 3*c*

FIG. 3.—Phase portraits of the three generic possibilities for flow near the upstream sonic point, C. Direction of the flow is indicated by arrows. All results were obtained by numerical integration of eq. (3.14), with $\eta = 45°$ and $\phi = 60°$. For this choice of η and ϕ, the critical values of α are $\alpha^{-}_{\rm crit} = 0.300$ and $\alpha^{+}_{\rm crit} = 6.67$. (*a*) Phase portrait for $\alpha = 0.25$, representing the case where C attracts the subsonic flow and a family of trajectories passes continuously from the subsonic into the supersonic region without being absorbed by the $M = 1$ line. The envelope of this family consists of the two special trajectories $\hat{\theta}_1$ and $\hat{\theta}_2$, which are drawn as dashed lines. The shaded portion of the figure is the unphysical region of phase space, as in Fig. 1. (*b*) The phase portrait for $\alpha = 0.5$, which illustrates the flow when no transonic trajectories exist. (*c*) Phase portrait for $\alpha = 10$, showing the case where C attracts the supersonic flow. Trajectories between $\hat{\theta}_1$ and $\hat{\theta}_2$ pass continuously into the subsonic region without being absorbed by $M = 1$.

viscous subshock to another trajectory with $\pi + \hat{\theta}_1 \leq \theta \leq \pi + \hat{\theta}_2$. Thus the flow in $\theta > \hat{\theta}_2$ represents J shocks. Trajectories inside the cone $\hat{\theta}_1 \leq \theta \leq \hat{\theta}_2$ (part of the "domain of attraction" of $\hat{\theta}_1$) comprise a new class of solutions, called C* shocks (C87), in which the gas is accelerated continuously through the sonic point. While local analysis cannot predict whether the solution for given boundary conditions is of type C*, it is significant that $\hat{\theta}_1$ has a domain of attraction with nonzero measure, because it suggests a nonzero probability for finding C* shocks for *some* choice of boundary conditions. In fact, the numerical calculations described below show that C* shocks are found in a variety of realistic problems.

ii) *The Downstream Sonic Point, C′*

As shown in Appendix B, there are always exactly two special transonic trajectories $\hat{\theta}_1$ and $\hat{\theta}_2$ at the downstream sonic point. For J or C* shocks with $M > 1$ at D, the solution trajectory must emerge from C′ along $\hat{\theta}_1$, where

$$\tan \hat{\theta}_1 = \frac{\sin \eta + \alpha \cos \eta - W^{1/2}}{2 \cos \eta} . \tag{3.17}$$

The phase portrait, given in Figure 4, shows that the C′ is a saddle point, as noted by Chernoff (C87). The numerical methods described in § IV make use of the divergent subsonic flow and convergent supersonic flow in the vicinity of C′.

c) Global Analysis

The numerical methods described in § IV rely upon three properties of the solutions to equation (3.8), which follow from Chernoff's analysis (C87), the analysis presented above, and the assumptions on which both are based. The latter are, specifically, that the fractional ionization remains low enough to make equation (3.8) a useful approximation to the hydrodynamics, and that the $R = 0$ and $M = 1$ curves in Figure 1 intersect in the manner shown. The first solution property, which was demonstrated by Chernoff, gives a practical method for classifying the shock structure as type C, J, or C*. It follows simply from the observation that

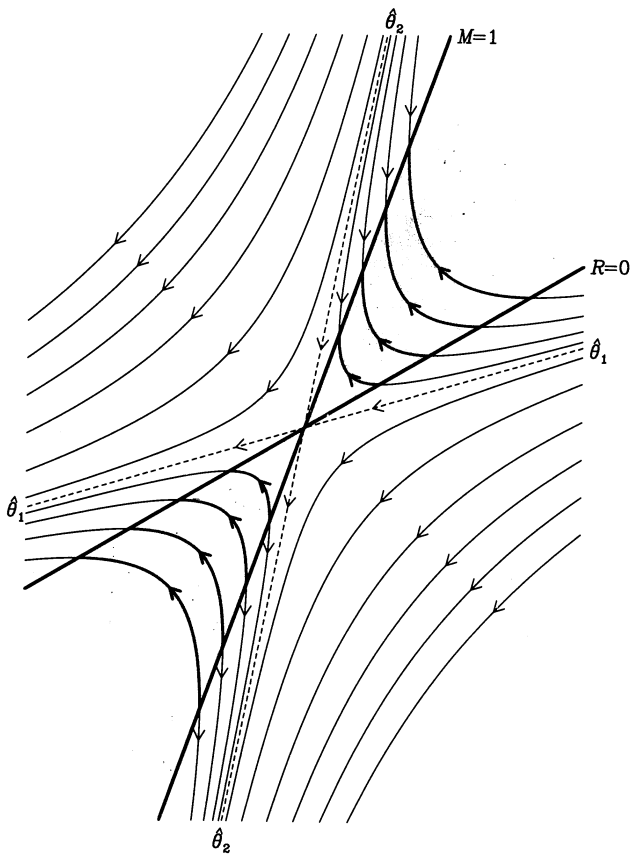

FIG. 4

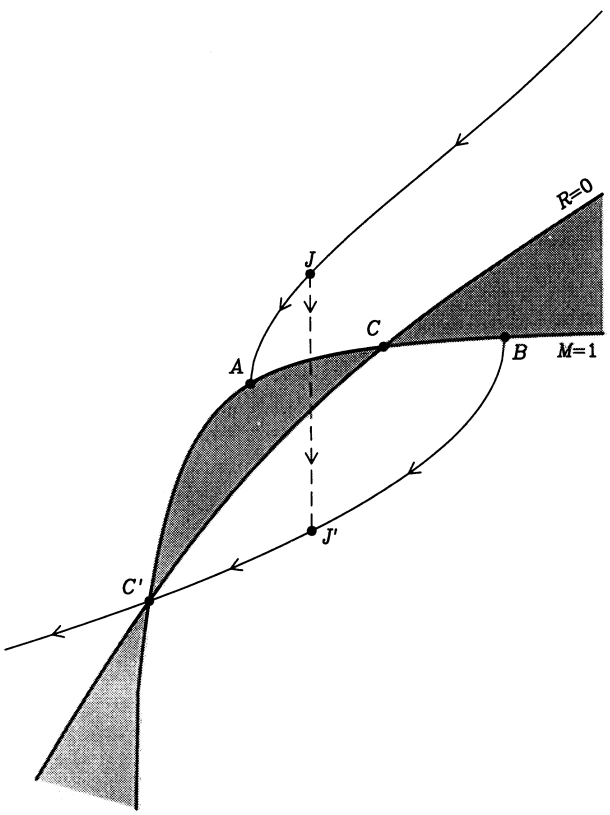

FIG. 5

FIG. 4.—Similar to Fig. 3, but for the downstream sonic point C′. Results shown here correspond to $\phi = 30°$, $\eta = 70°$, and $\alpha = 1$. Trajectory $\hat{\theta}_1$ (*dashed line*) is the only curve that passes smoothly into the supersonic region, and therefore corresponds to the solution curve for J or C* shocks that are supersonic at point D.

FIG. 5.—A sketch of phase space showing the essential steps in computing a J shock. The initial trajectory UJA (U not shown) terminates on $M = 1$, signaling the presence of a J shock. One next must locate a point J (assumed unique) such that an adiabatic discontinuity JJ′ connects UJA to BJ′C′, the unique subsonic trajectory that reaches D via C′. In flows with chemistry, this unique subsonic trajectory is not known *a priori* and must be determined by trying different choices of J: for each choice of J, one locates J′ using the jump conditions (3.9)–(3.10), and then integrates downstream from J′ (using a shooting procedure) until either reaching the sonic point C′ or failing; depending upon the failure mode (see text), a new trial choice of J is made, until the jump and the subsonic trajectory have been determined to sufficient precision. Having found the subsonic trajectory which reaches C′, one resumes the initial value integration on the subsonic side of C′, continuing until reaching D.

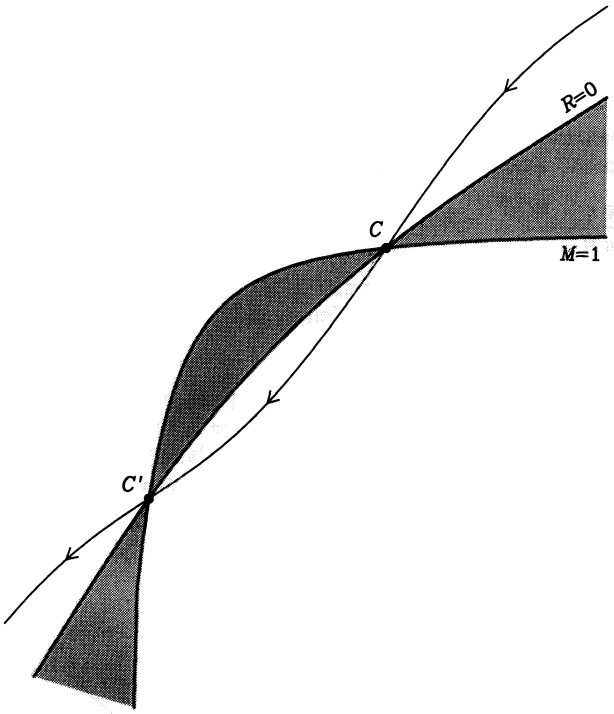

FIG. 6a

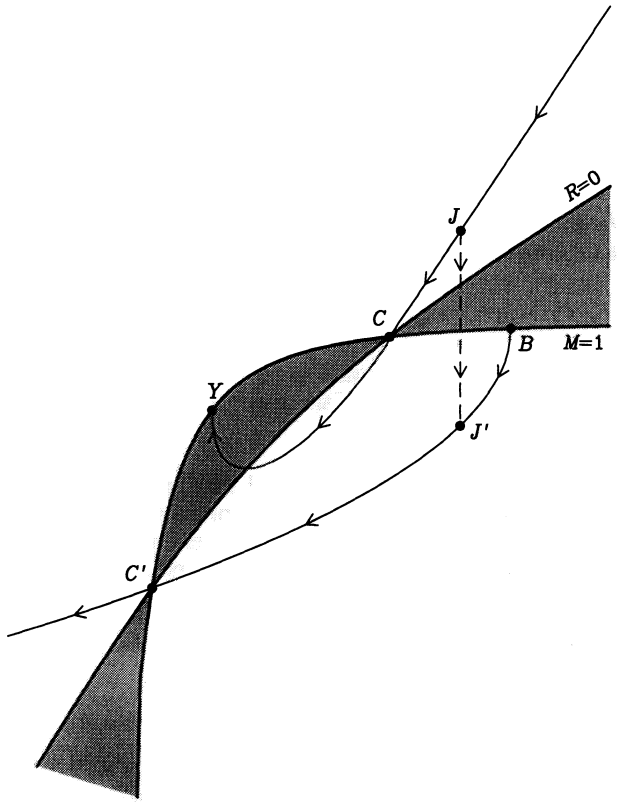

FIG. 6b

FIG. 6.—The essentials of computing a C* shock. The possibility of such a shock is signaled when the initial trajectory UC (U not shown) terminates at the sonic point C. One then extrapolates through C into the subsonic region, using the technique described in § IV*c*. Succeeding steps proceed as in the case of a J-type shock. If a subsonic trajectory can be found which reaches the downstream sonic point C′, then the solution is a C* shock, as shown in (*a*). If all subsonic trajectories emitted by C terminate with failure mode "*P*", then the shock is actually J-type, as shown in (*b*).

a trajectory starting from U can have only three possible outcomes. (1) If it reaches D without crossing the $M = 1$ line, then the shock is C-type. This possibility will not be considered further. (2) Alternatively, the trajectory may reach a point on $M = 1$ where $dv_n/dz = -\infty$ (point A in Fig. 5). This outcome implies that the shock is J-type—the solution can reach D only via an adiabatic jump, JJ′, from some (as yet unknown) point J on UJA to a subsonic trajectory BJ′C′D that reaches the downstream equilibrium state. (3) The final possibility is that the trajectory starting at U reaches point C, where dv_n/dz is finite. The preceding analysis, in which it was seen that C may be an attractor, shows that this outcome is a realistic possibility.

When a trajectory from U is able to reach C, there are two generic possibilities, given that the flow must "find" the unique trajectory passing from the subsonic region through C′. This unique trajectory, if integrated "backward" from C′, must either connect to the sonic point C (as in Fig. 6*a*), or it must terminate on the $M = 1$ curve to the right of C (as in Fig. 6*b*).[1] In the first case (Fig. 6*a*), termed a C* shock, the flow moves along the continuous trajectory from U to C to C′. In the second case (Fig. 6*b*), the flow must undergo a viscous subshock upstream from C in order to "jump" downward[2] onto the trajectory connecting to C′, and the solution is classified as J-type.

A second property used below is that the subsonic portion of a solution (BJ′C′ in Figs. 5 and 6*b* for a J shock, or CC′ in Fig. 6*a* for a C* shock) is unique. Appendix B shows that C′ is a repeller, and a unique trajectory passes through the subsonic region and into C′, so the assertion of uniqueness can be violated only if nonunique solutions join at some point upstream from C′. This requires, in turn, that the slope dr/dq must be multivalued at the point of intersection, in contradiction to expression (3.8). A corollary of this property is that C* solutions are unique. To see this, assume to the contrary that at least one additional solution can be found. The preceding discussion rules out the possibility that the second solution is a J shock, because the subsonic trajectory reaching C′ terminates at C (and therefore does not exist for $q > q_C$) and the supersonic trajectory terminates at C (and therefore does not exist for $q < q_C$), so a jump connecting supersonic to subsonic trajectories (at constant q) is not possible.[3] The only remaining possibility for nonuniqueness, the existence of two C* solutions, can also be ruled out: since the entire trajectory UCC′ is unique by the preceding arguments, the nonunique solutions must bifurcate between C′ and D. But since dr/dq is unique between C′ and D, this is impossible.

[1] By observing that $R > 0$ but $Q = 0$ on the $q = r$ line in this region, it is obvious that the trajectory passing though C′ cannot touch the $q = r$ line in the subsonic region. Similarly, this trajectory cannot touch the $R = 0$ line in the subsonic region.

[2] It is easy to show that such a jump is always possible when a trajectory UC exists and the trajectory reaching C′ passes below C.

[3] Note that the initial trajectory is unique even though dr/dq is multivalued at U, because physical considerations dictate a unique choice for dr/dq there. That is, one chooses the initial trajectory to be the fastest growing eigenmode of the linearized flow field at U (see D80).

It does not appear possible to demonstrate the uniqueness of J-type shocks using general mathematical arguments alone. For example, consider the curves $r_{UA}(q)$ and $r_{BC'}(q)$ in Figure 5, in the neighborhood of the points J and J′ (where $q = q_J$) which, by hypothesis, may be connected by an adiabatic jump. Suppose that in a finite interval $[q_1, q_2]$, with $q_1 < q_J < q_2$, the curves have the property $r_{UA}(q)/r_{BC'}(q) = constant$. Suppose further that the neutral Mach number and adiabatic index of the supersonic fluid are constant for $q \in [q_1, q_2]$. Then, since the compression ratio (the ratio $r_J/r_{J'}$) depends only on M and the adiabatic index, there are infinitely many solutions in this example, corresponding to jumps connecting UA and BJ′ at every point with $q_1 < q < q_2$.

Another characteristic of solutions used below is related to the uniqueness of the subsonic part of the solution. It is the fact that, for J-type and C* shocks respectively, BJ′C′ and CC′ divide the subsonic region into two disjoint sets of points: Points above either of these curves lie on trajectories that fail to reach D, because they cross $R = 0$, enter the region where $dv_n/dz > 0$, and flow upward to be absorbed by $M = 1$ (see Fig. 3). Similarly, points below the subsonic part of the solution are on trajectories that never reach D, because they eventually cross $q = r$, where dv_i/dz changes sign. The utility of this property is that, given a trajectory that has failed to pass through C′, the mode of its failure, with $dv_n/dz > 0$ (henceforth called "mode P"), or with $v_n < v_i$ (henceforth called "mode N") tells whether the failed trajectory lies above or below the solution curve. This is the basis of the shooting technique described below, which is used to refine subsonic solutions in § IV. It is also the basis of the method used to distinguish between C*- and J-type shocks in those cases where trajectories exist connecting U to C. Consider a very small region containing C, and consider trajectories originating on the subsonic boundary of this small region. If every trajectory fails with mode P, then we know that the trajectory which reaches C′ must pass below the sonic point C and can be reached only by an adiabatic jump. If, on the other hand, one can find a trajectory with failure mode N, then one is assured that the flow is C*-type.

d) When Do C Shocks Occur?*

We have discussed above the different types of shocks which can occur and the methods used to classify a particular solution. It is of course of great interest to know under what circumstances different types of shocks occur. Within the approximation of the phase portrait description adopted here, the character of a shock solution is determined entirely by the "Alfvén Mach number" M_{nA} and the "heating-cooling function" $H_n(r, t)$. Chernoff (1987) has investigated the nature of the solutions found for various power-law functions H_n, and he finds C* solutions to be relatively uncommon. Real cooling functions of interstellar gas are, however, often characterized by a rapid decrease in cooling when the temperature falls below some "threshold" value T_{thresh}, where kT_{thresh} is the energy required to excite the first excited state with a large enough radiative decay rate to produce significant cooling. We therefore consider cooling functions of the general form

$$\Lambda = A\rho_n^m T_n^\beta \exp\left(-T_{thresh}/T_n\right), \tag{3.18}$$

where Λ is the power radiated per unit volume, and A, m, β, and T_{thresh} are constants. It is convenient to define the dimensionless "threshold parameter"

$$\theta \equiv \frac{4\pi\rho_{n0}\, kT_{thresh}}{\mu_n B_0^2}, \tag{3.19}$$

and the dimensionless "cooling strength parameter"

$$\lambda \equiv \rho_{n0}^{m-1}\left(\frac{\mu_n B_0^2}{4\pi\rho_{n0}\, k}\right)^{\beta-1} \frac{\mu_n(\mu_n + \mu_i)}{k\rho_{i0}\langle\sigma v\rangle} A\,. \tag{3.20}$$

With these definitions, the dimensionless heating-cooling function H_n has the form

$$H_n = -\lambda M_{nA}^{2\beta-2} t^\beta q r^{-m} \exp\left(-\theta/M_{nA}^2 t\right). \tag{3.21}$$

Note that for fixed preshock conditions (ρ_{n0}, ρ_{i0}, B_0, μ_n, and μ_i) and fixed cooling function parameters (A, T_{thresh}, m and β), the parameters θ and λ are constant. It is convenient to characterize the magnetic field in the preshock gas by the dimensionless parameter $b_0 \equiv (B_0/\mu G)(n_H/\mathrm{cm}^{-3})^{-1/2}$; interstellar clouds with $n_H \gtrsim 10\ \mathrm{cm}^{-3}$ appear to have $b_0 \approx 1$ (Troland and Heiles 1986). The cooling threshold parameter is then $\theta = 0.867 b_0^{-2}\,(T_{thresh}/500\ \mathrm{K})(1.1 - n[H_2]/n_H)^{-1}$. Thus, for cooling by the $J = 2 \rightarrow 0$ transition of H_2 ($T_{thresh} = 510$ K), $\theta \approx b_0^{-2}$; because of the small Einstein A coefficient for this transition, larger J levels are often important (e.g., $J = 3 \rightarrow 1$, $T_{thresh} = 845$ K), and H_2 rotational cooling will typically be characterized by a somewhat larger value of θ. In higher velocity shocks, vibrational excitation of H_2 will make an important contribution to the cooling; with $T_{thresh} = 6000$ K, $\theta \approx 10 b_0^{-2}$ would be indicated. However, vibrational cooling of H_2 will generally be accompanied by rotational cooling which "turns on" at lower temperatures, so that $\theta \approx 5 b_0^{-2}$ is probably a good representative value to consider.

Chernoff (1987) computed shock solutions for cooling functions of the form $H_n = -\Psi_0 q^a r^{b-1} t^{c+1}$, with a, b, c (Chernoff's α, β, γ), and Ψ_0 constant. As seen above, however, except for the special case $\beta = 1$ (i.e., $c = 0$), the cooling function H_n should include an explicit dependence on the Alfvén Mach number M_{nA}. Therefore, Chernoff's shock solutions for constant Ψ_0, a, b, c, and varying M_{nA} do *not* represent a series of shocks with constant preshock conditions and varying shock speed.

With a cooling function of the form of equation (3.21), the nature of the shock is fully determined by the five parameters M_{nA}, λ, θ, β, m, and γ; in the present discussion, we will fix $m = 2$ (appropriate for low densities), $\beta = 1/2$ (which gives a reasonable approximation to several different realistic coolants), and $\gamma = 5/3$ (monatomic gas, or molecular gas at low densities). We have computed a number of shock solutions for selected values of the remaining free parameters λ, θ, and M_{nA}. In Figures 7*a* and 7*b*, we show the domains (on the $M_{nA} - \lambda$ plane) of different classes of solutions, for two choices of the threshold parameter: $\theta = 2$ and $\theta = 5$.

In the course of obtaining shock solutions for the cooling function (eq. [3.21]), it was discovered that in a significant fraction of cases there were four "sonic points" where the $R = 0$ and $M = 1$ curves intersected. Denote these, in order of decreasing q, as C_1,

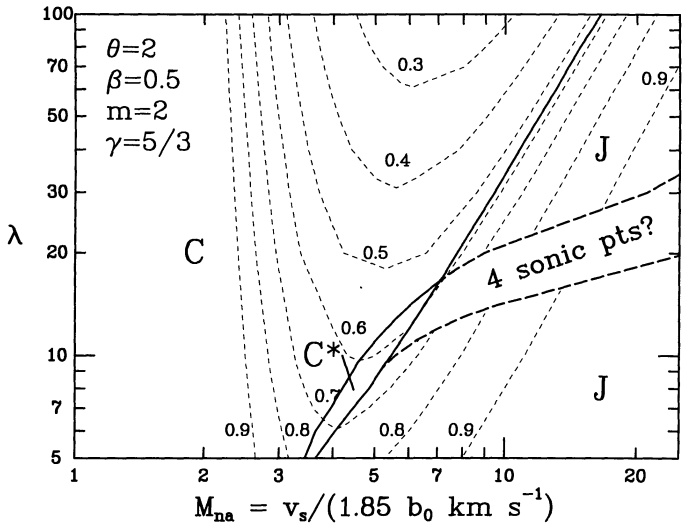

FIG. 7a

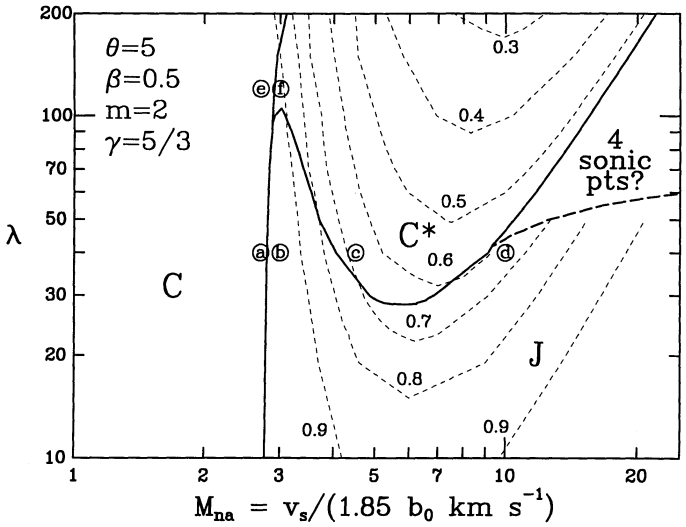

FIG. 7b

FIG. 7.—Classification of shock solutions for flows with a cooling function of the form $\Lambda = A\rho_n^2 T_n^{0.5} \exp(-T_{\rm thresh}/T_n)$, for a $\gamma = 5/3$ gas. Solutions are classified by the "Alfvén Mach number" M_{nA}, the "threshold" parameter θ, and the "cooling strength" parameter λ, defined by eqs. (3.18)–(3.21) (see text). Classifications shown here are for (*a*) $\theta = 2$ and (*b*) $\theta = 5$; in each case, solution space is divided into four regions. In three of these regions, the flow trajectory has either zero or two sonic transitions, and the shocks are either C-type, C*-type, or J-type. In the fourth region, labeled "4 sonic points?," the flow trajectory could have as many as four sonic transitions, and solution classification has not been attempted. Also plotted on each figure are contours (*dashed lines*) of constant $T_{\rm max}/T_{\rm ad}$, where $T_{\rm max}$ is the maximum temperature attained by the neutral gas and $T_{\rm ad}$ is the postshock temperature in a flow with the same value of M_{nA} but no cooling; contours are labeled by $T_{\rm max}/T_{\rm ad}$. In (*b*) are shown the locations of the six shocks (*a–f*) for which phase portraits are shown in Fig. 8 below.

C_1', C_2, and C_2'. Sonic points C_1 and C_2 are of the type referred to above as "upstream," and they may attract supersonic flow. Sonic points C_1' and C_2', through which trajectories may pass from the subsonic to supersonic regions, are of the type referred to above as "downstream."

When four (or more) potential sonic points exist and the shock trajectory is not C-type, the analysis and classification of the shocks can be more complicated than for the two–sonic-point case discussed above. Suppose that there are exactly four potential sonic points C_1, C_1', C_2, C_2', located at $q = q_1 > q_2 > q_3 > q_4$. If the trajectory beginning at U remains supersonic ($M > 1$) throughout $q \geq q_2$, then the flow itself must make either zero or two sonic transitions, and classification as C-, C*-, or J-type proceeds just as described above. If, however, the trajectory beginning at U intersects the $M = 1$ curve between q_2 and q_1, or if it reaches sonic point C_1, then the flow trajectory can have either two or four sonic transitions; such shocks occur in the regions labelled "4 sonic points?" in Figures 7*a* and 7*b*. For example, it is possible in principle to have a shock solution which passes smoothly through the sonic point C_1, returns to supersonic flow through C_1', makes a jump across the $M = 1$ line back to subsonic flow, and finally returns to supersonic flow through C_2'. Because of this complexity, we will defer detailed discussion of such transonic flows to a later paper; the discussion of the present paper will be restricted to flows with zero or two sonic points.

Figures 7*a* and 7*b* show that the topology of solution space is complex and sensitive to the detailed behavior of the cooling function. In the $\theta = 2$ shocks of Figure 7*a*, C* shocks exist in only a small fraction of the parameter space surveyed and might be regarded as a relatively unimportant curiosity. In the $\theta = 5$ shocks of Figure 7*b*, however, the C* solutions occupy a very substantial portion of parameter space.

To illustrate the importance of cooling, on Figures 7*a* and 7*b* we plot contours of constant $t_{\rm max}/t_{\rm ad}$, where $t_{\rm ad}$ is the temperature which would be attained in a shock with the same preshock parameters and shock speed, but no radiative cooling; $t_{\rm ad}$ may be evaluated by first computing the postshock velocity $q_{\rm ad} = r_{\rm ad}$ in a nonradiative shock with $t_0 = 0$ (see Appendix C):

$$r_{\rm ad} = \frac{(\gamma - 1) + \gamma M_{nA}^{-2} + \{[(\gamma - 1) + \gamma M_{nA}^{-2}]^2 + 4(\gamma + 1)(2 - \gamma)M_{nA}^{-2}\}^{1/2}}{2(\gamma + 1)}, \tag{3.22}$$

and then using equation (3.5) to evaluate

$$t_{\rm ad}(M_{nA}) = r_{\rm ad}[1 + t_0 - r_{\rm ad} + \tfrac{1}{2}M_{nA}^{-2}(1 - r_{\rm ad}^{-2})], \tag{3.23}$$

which varies between 0 and $2(\gamma - 1)/(\gamma + 1)^2 (= 3/16$ for $\gamma = 5/3)$ as M_{nA} varies from 1 to ∞.

The exponential factor $\exp(-\theta/M_{nA}^2\, t)$ will strongly suppress the cooling rate in all models with $M_{nA}^2\, t_{\rm ad}(M_{nA}) < \theta$. For $\gamma = 5/3$, $M_{nA}^2\, t_{\rm ad} < 2$ for $M_{nA} < 3.99$, and $M_{nA}^2\, t_{\rm ad} < 5$ for $M_{nA} < 5.72$. This explains why $t_{\rm max}/t_{\rm ad} \to 1$ as $M_{nA} \to 1$ in Figures 7*a* and 7*b*. We see that in the shock solutions shown in Figures 7*a* and 7*b*, there are values of λ and M_{nA} where the peak temperature $t_{\rm max}$ attained in the flow is small compared to the value $t_{\rm ad}$, which would apply if the ion and neutral fluids were strongly coupled and treated as a single fluid.

For $\theta = 2$ (see Fig. 7*a*), we observe that for $4 \lesssim \lambda \lesssim 15$, as one increases M_{nA} (beginning from $M_{nA} = 1$) one first obtains C-type shocks, then C* shocks, and finally J shocks. For $\lambda \gtrsim 15$, C* shocks do not occur, and one goes from C shocks at small M_{nA} to J shocks at large M_{nA}. These solution sequences are in accord with those found by Chernoff (C87) for power-law cooling functions.

For $\theta = 5$, however, the situation is quite different (see Fig. 7*b*): for $20 \lesssim \lambda \lesssim 100$, as we increase M_{nA} from small values we first obtain C solutions, then a range of J shocks, then a range of C* shocks, and finally J shocks prevail for large M_{nA}.

To understand why these two different sequences (C-J-C*-J vs. C-C*-J) occur, we present phase portraits of six exemplary shocks in Figure 8, all for a cooling function with $\theta = 5$. The phase portraits show the solution trajectory, the $R = 0$, $M = 1$, and $q = r$ curves, and also contours of constant t/t_{ad} (*dashed lines*), for $t/t_{ad} = 0$, 0.25, 0.5, 0.75, and 1. Before considering specific realizations, we note that the solution trajectory must lie within the "envelope" defined by the $t/t_{ad} = 0$ and $t/t_{ad} = 1$ contours, because the neutral fluid temperature must be nonnegative and must remain below the maximum value which would be attained in a fully

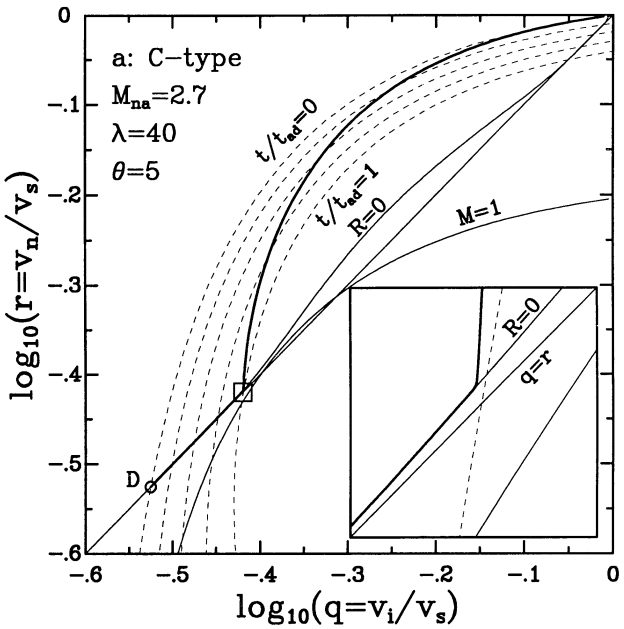

FIG. 8*a*

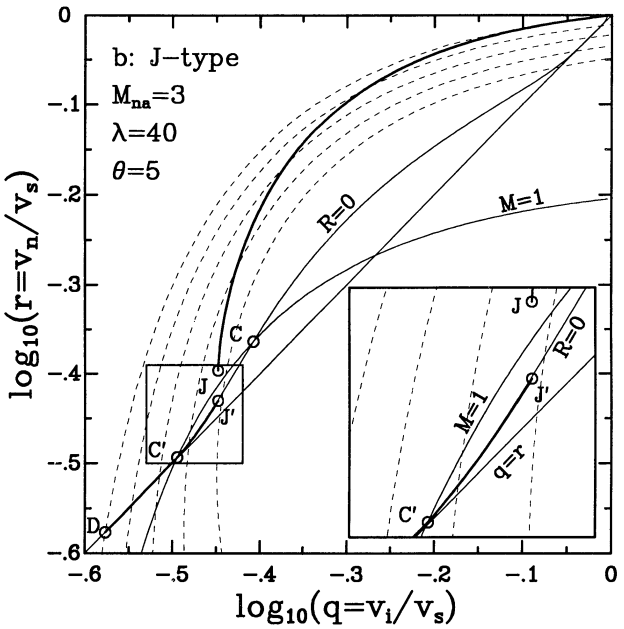

FIG. 8*b*

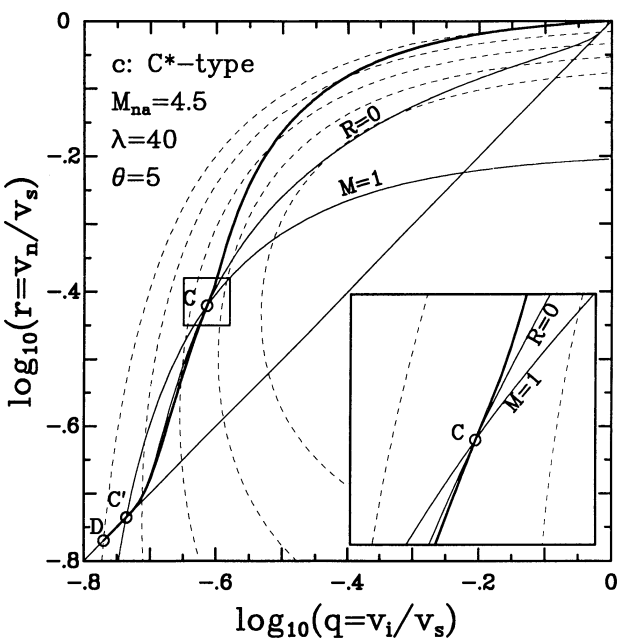

FIG. 8*c*

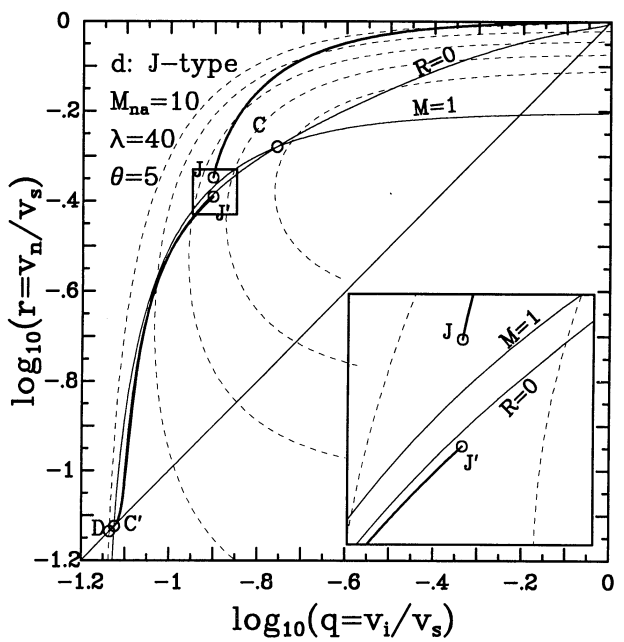

FIG. 8*d*

FIG. 8.—Phase portraits for six exemplary shocks with a cooling function of the form $\Lambda = A\rho_n^2 T_n^{0.5} \exp(-T_{thresh}/T_n)$, for a $\gamma = 5/3$ gas. All examples shown are for cooling threshold parameter $\theta = 5$. In each portrait, the heavy curve is the solution trajectory. Also shown are the $q = r$, $M = 1$, and $R = 0$ curves, as well as contours of $t/t_{ad} = 0$, 0.25, 0.5, 0.75, and 1 (*dashed lines*), where t_{ad} is the dimensionless temperature which would be attained for each shock in the absence of cooling. In each portrait, there is an inset showing an expanded view of a portion of the phase trajectory. (*a*) C-type shock with $\lambda = 40$, $M_{nA} = 2.7$; (*b*) J-type shock with $\lambda = 40$, $M_{nA} = 3$; (*c*) C*-type shock with $\lambda = 40$, $M_{nA} = 4.5$; (*d*) J-type shock with $\lambda = 40$, $M_{nA} = 10$; (*e*) C-type shock with $\lambda = 120$, $M_{nA} = 2.7$; (*f*) C*-type shock with $\lambda = 120$, $M_{nA} = 3$.

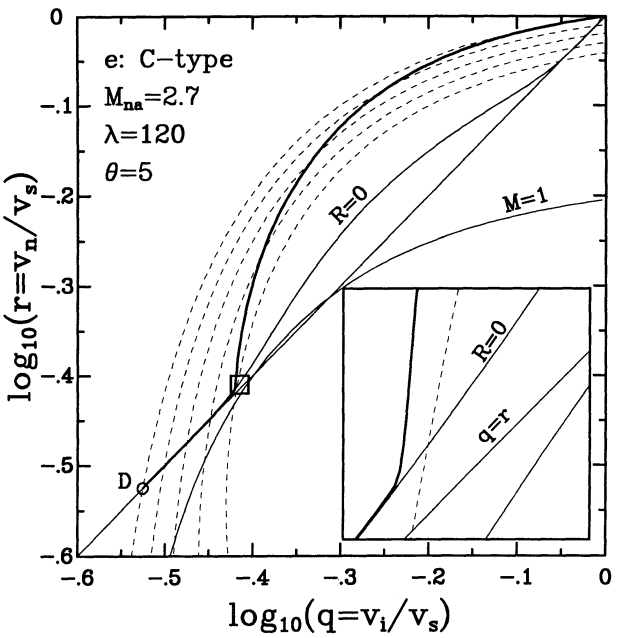

FIG. 8e

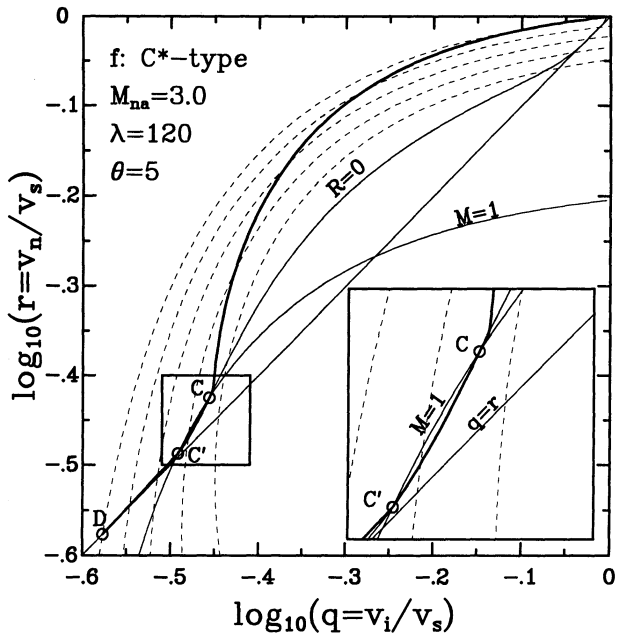

FIG. 8f

adiabatic shock. If cooling is strong, the trajectory will tend to remain on the "cold" side of the envelope; if cooling is weak, then the trajectory (which starts on the "cold" edge of the envelope at U) gradually moves toward the "hot" side of the envelope (though it cannot actually reach the hot side of the envelope except at $q = r$). Note that this "envelope" is independent of the nature of the cooling function; it depends only on M_{nA}.

Figure 8*a* shows a C-type shock model for $M_{nA} = 2.7$. Cooling is relatively unimportant until the trajectory approaches close to the $q = r$ line; at this point, heating by ion-neutral friction becomes small and remains small as the fluid slowly cools until it reaches point D. This shock would be C-type even in the absence of cooling.

If we now increase the shock speed to $M_{nA} = 3$, both the $M = 1$ and $R = 0$ curves move upward in the plot (see Fig. 8*b*), and the upstream solution trajectory would terminate on the $M = 1$ curve if continued; the upstream trajectory therefore terminates at the point J where the neutral fluid undergoes a viscous subshock and the solution trajectory "jumps" to point J′ below the $R = 0$ curve; from J′, the trajectory continues through the downstream sonic point C′ and terminates at D. Note that the latter part of the solution trajectory lies very close to the $R = 0$ curve, which, because of the strong exponential suppression of the cooling function at low temperatures, is itself very close to the $q = r$ curve downstream from C′.

Further increasing the shock speed to $M_{nA} = 4.5$ (Fig. 8*c*), we find that the $R = 0$ and $M = 1$ curves have moved to new positions such that the upstream solution trajectory "descends" (within the "thermal envelope") to the right of the sonic point C and approaches the $R = 0$ curve. The trajectory (which cannot cross the $R = 0$ curve) is "channeled" by the $R = 0$ curve to the neighborhood of the sonic point C, which in this case attracts supersonic flow. The trajectory passes through C (see inset in Fig. 8*c*) into the subsonic region and through the subsonic region to the downstream sonic point C′, through which it passes to reach D. This is an explicit example of a C*-type shock.

Further increasing the shock speed to $M_{nA} = 10$, we obtain another example of J-type shocks: the upstream trajectory descends toward the $M = 1$ curve, so it must jump from J to J′ and then through C′ to D. Figures 8a–8d provide an explicit set of models exhibiting the C-J-C*-J sequence of shock types as M_{nA} is increased.

To see how the sequence C-C*-J can occur, we turn to Figures 8*e* and 8*f*, which show solutions for $\lambda = 120$—cooling 3 times stronger than the models of Figures 8*a*–8*d*. Figure 8*e* shows a C shock which has a phase portrait quite similar to that of Figure 8*a*, the main difference being that the $R = 0$ curve moves farther away from the $q = r$ line. Increasing M_{nA} from 2.7 to 3 results in the C* shock of Figure 8*f*. What happens here is that as M_{nA} is increased, the $M = 1$ curve moves upward and intersects the $R = 0$ curve in such a way that both sonic points (C and C′) lie to the left of the descending upstream trajectory. The upstream trajectory is therefore "channeled" by the $R = 0$ curve into the neighborhood of the attractor C. We note that in this case the effects of cooling are relatively minor as far as the upstream flow is concerned (comparison of Figs. 8*b* and 8*f* shows that the upstream trajectories are nearly indistinguishable): the primary effect of changing the cooling (changing λ from 30 to 120) is to shift the $R = 0$ curve and the sonic points C and C′, thereby forcing a dramatic change in the type of shock solution which is possible.

The main lesson to be drawn from these examples, and from the complex solution topology of Figures 7*a* and 7*b*, is that only a detailed analysis will show which type of solution will occur when strong cooling is possible.

IV. NUMERICAL METHODS

a) The Forward Integration Step

The methods used below to calculate J-type and C* solutions have in common a basic step, in which equations (2.1)–(2.6) are integrated forward over some spatial interval, say from z_1 to $z_1 + \Delta z$. In carrying out this step, our calculations employ the

following expedient for reasons of computational efficiency: from the chemical source terms, C_j, at point z_1 we evaluate the length scale Δz_{ch} over which the most rapidly varying chemical flux will change by some predefined amount, typically 10%. We then fix the fluxes $n_j v_j$, of all chemical species except H_2, at the values which pertain to z_1 and take a "hydrodynamics step" of length Δz_{ch}. In this step, we integrate equations (2.1)–(2.5), plus an additional equation for $dn(H_2)/dz$, from z_1 to $z_1 + \Delta z_{ch}$. The numerical integration is carried out using Gear's quadrature method for stiff equations (Gear 1971). The chemistry equations (2.6) are then integrated with a Runge-Kutta scheme from z_1 to $z_1 + \Delta z_{ch}$ in a "chemistry step," in which the spatial dependence of T_n and other hydrodynamical variables that affect the chemistry is obtained by linear interpolation in the results of the hydrodynamics step. Our chemical reaction network is divided into "slow" and "fast" species, where fast species are those molecular ions subject to rapid destruction by dissociative recombination. The fast species are assumed to have abundances as though in instantaneous equilibrium with the other chemical constituents. The reason for treating H_2 on a different footing from the other chemical variables is that, since H_2 is usually the dominant coolant in shock-heated gas, the hydrodynamical equations are strongly coupled to its abundance. After each chemical step, the stepsize Δz_{ch} is reevaluated and a new hydrodynamics step is taken; the whole process is repeated until all variables have reached $z_1 + \Delta z$.

b) *Numerical Methods for* J *Shocks*

Suppose that the initial trajectory has terminated at point A in Figure 5. To continue the integration, one must find the post-jump fluid variables at the unknown point J′ and integrate downstream through the sonic point, C′, to D. These steps can be carried out using different forms of "shooting," a standard method for solving two-point boundary value problems (see Press *et al.* 1986, chap. 16, for details). In our implementation, shooting guesses the unknown fluid variables at J′ and integrates downstream with the initial value methods described above. Shooting at J′ is particularly simple: Only the position z_J of the jump needs to be guessed, because the Rankine-Hugoniot jump conditions relate the postjump variables uniquely to their prejump values at z_J (Landau and Lifshitz 1959). As z_J converges to its correct value, the trial solutions are found to propagate closer and closer to C′ before diverging toward aphysical downstream boundary conditions.

If there is a unique J-type solution, then the following procedure is guaranteed to converge on z_J. Consider outcomes of trial solutions with various guesses, $\tilde{z}$, at z_J. As $\tilde{z}$ moves along the initial trajectory toward A, the neutral Mach number decreases to unity and, according to the Rankine-Hugoniot relations, the compression ratio across the jump front also approaches unity. Thus, if $\tilde{z}$ is too close to Λ, then the trial must fail with mode P defined above (see Fig. 5). This establishes an upper bound $z_J^P = \tilde{z}$ on z_J. Now consider a sequence of trials with progressively smaller guesses $\tilde{z} < z_J^P$. When the sequence reaches a value $\tilde{z} < z_J$, the trials must begin to fail with mode N. This establishes a lower bound, z_J^N, on z_J. Once the bounds have been established, a "binary chop" procedure can be used to refine the guesses with arbitrary accuracy.

In practice, however, the degree of refinement which can be attained using binary chop is limited by the finite precision with which the calculations are always performed. As a result, the trial solutions can never be propagated through the divergent flow at the saddle point, C′. Since the trial integrations require substantial amounts of computation, we usually abandon the binary chop procedure when z_J has converged to four or five significant digits. At this point the calculations have yielded two trajectories that have terminated upstream from C′, with opposite failure modes. In our models, we accept, as valid approximations to the true solution, all variables that differ by less than some tolerance, typically one percent, between the two failed trajectories. This generally yields solution values for the flow between J′ and some point Y, upstream from C′, where the tolerance criterion is not satisified.

To proceed, shooting must be used to propagate the variables downstream from the new shooting point, Y. The shooting procedure to be adopted is ambiguous, however, because there are several variables to refine and only one constraint to satisfy: that the solution should propagate closer to C′ before failing. In our calculations, we use phase space averaging: mean values of variables on the two failed trajectories at Y yield an "averaged trajectory," which is then propagated downstream using the initial value method. The averaged trajectory then replaces one of its progenitors, depending on its failure mode. The whole procedure is repeated, advancing the shooting point toward C′ whenever the variables have converged to the required tolerance. The discussion of § III*c* shows that, in a two-dimensional phase space, the averaged trajectory is trapped between the failed trajectories which, in turn, bracket the desired solution. It follows that averaging is guaranteed to converge in systems where the hydrodynamics and chemistry are uncoupled; the applicability of this approach to realistic systems is discussed in § IV*d*.

The preceding steps yield two divergent trajectories that have approached point C′ (Fig. 4). The phase flow divergence close to C′ eventually makes averaging impractical, and this method is abandoned at a point where, typically, the neutral Mach number is $M \approx 0.90$–0.99. Figure 4 shows that the phase flow converges *downstream* from C′, so that the downstream supersonic solution will be insensitive to small errors in the procedure used to propagate through C′. Our calculations extrapolate into the supersonic region by replacing the singular differential equation (2.1) with

$$\frac{dv_n}{dz} = \frac{dr}{dq} \times \frac{dv_i}{dz}, \tag{4.1}$$

where dv_i/dz is determined by equation (2.2) and dr/dq is a constant, determined as follows: We find, by trial and error, that value of dr/dq that allows extrapolation to propagate from the last accepted solution point into and across the sonic point. The justification for this procedure is that, according to Figure 4, the physically relevant trajectory through C′ has dr/dq = constant for points sufficiently close to C′. We abandon the extrapolation typically when $M \simeq 1.01$ and resume integration of equations (2.1)–(2.6). Because the extrapolation is always small, in the sense that the fluid variables change by small amounts, our solutions are insensitive to the details of this procedure.

c) *Numerical Methods for* C* *Shocks*

Most of the preceding discussion carries over to the calculation of C* shocks, the exception being the method used to propagate through the upstream sonic point (Fig. 6*a*). Since C attracts trajectories, the initial value integration of equations (2.1)–(2.6) can be

carried quite close to C; in our calculations, the initial trajectory terminates when $M - 1 < \epsilon$, where $\epsilon \sim 10^{-3}$. If a jump front inserted at this point fails with mode N, then one is assured that the correct solution is either a C* shock or an extremely weak J shock. We ignore the distinction between these two outcomes, because in the latter case the shock compression ratio must differ from unity by a factor of order ϵ.

To proceed, some form of extrapolation must be used to carry the solution into the subsonic region. A reasonable approach might be to use L'Hôpital's Rule to evaluate the rational expression on the right-hand side of equation (2.1), as in the derivation of equation (3.14). In fact, we have found this strategy to be successful in only a small fraction of the shock models we have computed, for two reasons. First, to the extent that L'Hôpital's Rule faithfully reproduces the phase flow in Fig. 3*c*, it yields trajectories that rapidly diverge from the desired solution on the downstream side of C. Thus, unless they are computed with extremely high precision, trajectories obtained with L'Hôpital's rule will fail any reasonable accuracy criterion after propagating a short distance past C. One then has the problem that the shooting procedure for the subsonic flow, described below, converges very slowly. Second, L'Hôpital's Rule fails to yield smooth transonic trajectories when a weak J shock has been misclassified as a C* shock: The linearized flow field does not pass through C in such cases (Figs. 3*a* and 3*b*).

Our simulations rely on the observation that a C* shock may be regarded as a limiting case of the J shock shown in Figure 5, in which points A and B have converged on point C. It therefore follows that an arbitrarily good approximation to a C* solution can be obtained as the limit of a sequence of J shocks, in which the position of the jump front moves closer and closer to the sonic point. Of course, this limit cannot be carried out in practice—the best approximation that can be obtained is the weak J shock in which the jump has been inserted at the last computed point on the initial trajectory. Although this is usually a very good approximation, in the sense that the subsonic portion of the trajectory propagates a significant distance downstream before failing, it nevertheless must always fail with mode N. To continue, one must generate another trajectory, which fails with mode P, and shoot on the subsonic flow with the averaging method. To the extent that the two-dimensional phase space description is physically correct, the exact manner for obtaining the P-mode trajectory is unimportant. Our codes take the fluid variables at point J′ on the mode N trajectory, and replace v_i with $v_i + \delta v_i$, where $\delta v_i < 0$. Because J′ is close to point C, a small perturbation δv_i usually generates a mode P trajectory: typically $\delta v_i \sim 10^{-3}\ v_i$. Once the phase space averaging procedure begins, the calculation of a C* shock proceeds just as for a J shock.

d) Validity of the Underlying Assumptions

The numerical methods discussed above rely at several points on the two-dimensional phase space picture, in which chemistry decouples from the hydrodynamics. In practice, however, the methods are applied to problems in which the chemical evolution of the gas is followed via the reaction network (eq. [2.6]). It is natural to ask whether the methods are valid in such "multidimensional flows." In practice, the assumption of low fractional ionization can be satisfied by limiting the shock speed to sufficiently small values. The important question is whether the topology of curves in Figure 1 correctly describes the intersection of critical lines in shocks with chemistry.

In shocks with chemistry, one may still construct a picture like Figure 1, the only change being that, in addition to q and r, the curve $R = 0$ depends through H_n on values of the other "hidden" hydrodynamical and chemical variables. Suppose, for example, that Figure 1 was drawn using values of the hidden variables at the preshock state. Evolution of the solution (in z) can be visualized as a motion picture, in which the solution trajectory gradually propagates outward from U. Since the hidden variables depend on z, the curve $R = 0$ will in general move about as the picture evolves, allowing behavior of the solution trajectory that is not anticipated in the preceding discussion. In particular, the "motion" of $R = 0$ makes it possible, in principle, for the solution to cross $R = 0$, even though $\dot{r} = 0$ and $\dot{q} < 0$ on $R = 0$.

In fact, a simple argument suggests that this difficulty should not occur in simulations of diffuse cloud shocks. Consider a point where the solution trajectory has just reached the $R = 0$ line. Differentiation of equation (3.5) (which depends only on the assumption of low fractional ionization) with respect to z' implies that $\dot{t} = q - r$ when $\dot{r} = 0$. Since $q - r$ is always negative in the phase space region of physical interest, one sees that $dT_n/dz < 0$ wherever the solution curve touches $R = 0$. If the abundances of coolant species are not changing, and if the cooling rate $-H_n$ is a monotonic increasing function of T_n, which is usually the case, then H_n must be decreasing in magnitude when the solution reaches $R = 0$. This implies, in turn, that $R = 0$ must be moving *toward* the $q = r$ line and *away* from the solution curve (see eq. [3.8*b*]). Of course, the preceding conclusion might be incorrect if the coolant abundances are increasing rapidly at the point in question. However, the hot gas at such points is cooled mainly by H_2, whose abundance tends to *decrease* because of collision-induced dissociation. We conclude that the solution does not cross $R = 0$ in diffuse cloud shocks.

From the preceding argument, and the fact that the $M = 1$ curve is independent of H_n, it follows that our conclusions concerning the possible outcomes of the initial trajectory must be valid: The solution either reaches D (C shock), is absorbed by $M = 1$ (J shock), or flows through point C to C′ (C* shock). As a result, the derivation of equation (3.14) and its consequences remain valid for shocks with chemistry, because those consequences depend on the values of certain quantities at sonic points, but not on the history of a trajectory that happens to reach such a point. It should be noted, however, that convergence of the numerical methods is not guaranteed when chemistry is important. This is because the methods rely on the fact that trajectories in a two-dimensional system cannot intersect (except at sonic points and fixed points). In dimensions greater than two, aberrant behavior is possible (see Bender and Orszag 1978), although we have not encountered any aberrations in our calculations.

V. EXAMPLES

To test our numerical methods, we have computed a sequence of model shocks for shock speeds $v_s = 5$–30 km s^{-1} and other initial conditions as specified in Table 1. The models were computed using a realistic description of chemical, thermal, and other physical processes, as summarized in § II and described more fully in a future paper. Here we simply note that the abundance,

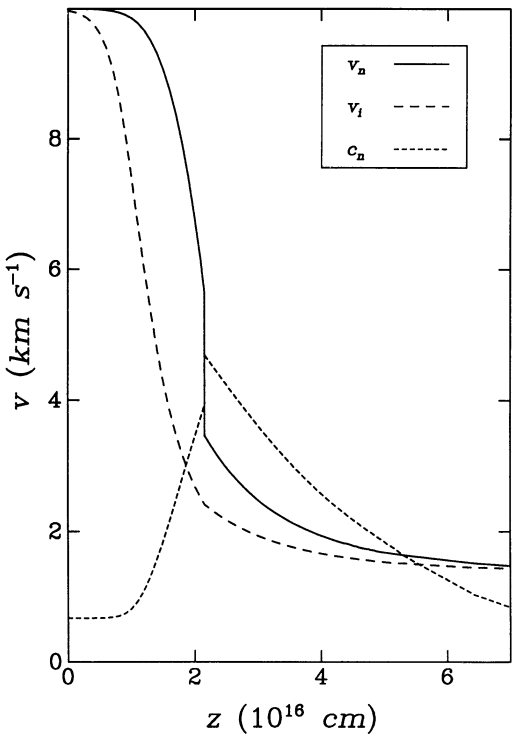

FIG. 9a

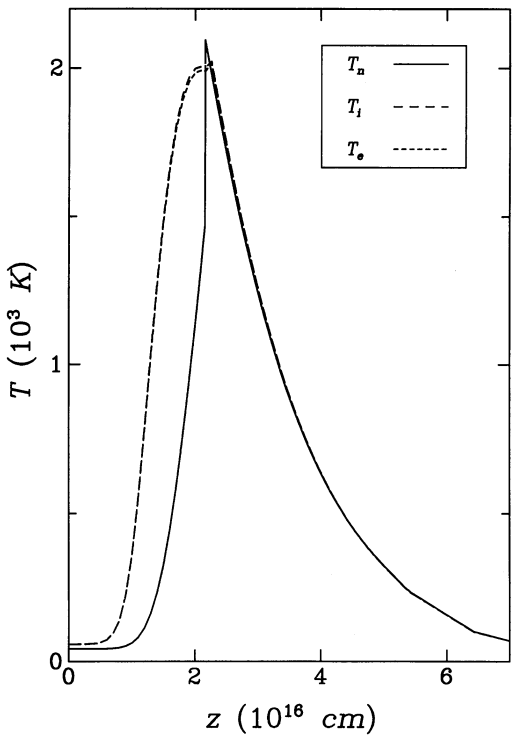

FIG. 9b

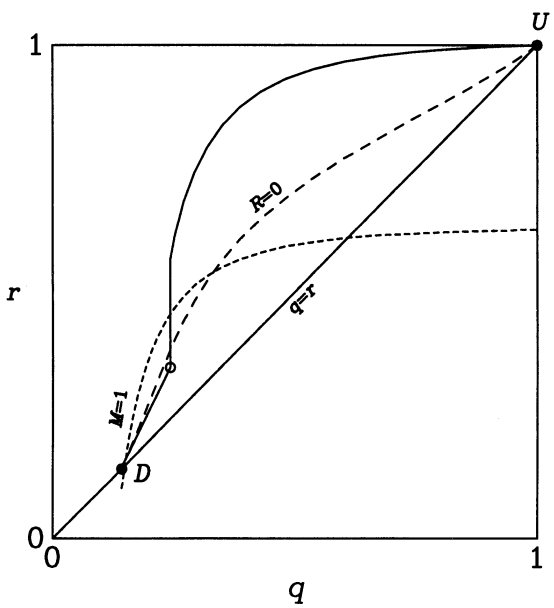

FIG. 9c

FIG. 9.—The result of applying our methods to calculate a J-type shock in a flow with heating, cooling, and chemistry. Parameters specifying the preshock conditions are given in Table 1. The shock speed was chosen to be 10 km s^{-1}. (*a*) Neutral velocity, ion velocity, and neutral sound speed as a function of position *z*. Compression ratio across the jump front is 1.6. (*b*) Neutral, ion, and electron temperatures vs. *z*. (*c*) Phase portrait of this shock. Open circle indicates the point where T_n attains its maximum value, which is 0.91 of the peak value which would have been attained in a single fluid shock, or in the absence of cooling. The line $R = 0$ is not strictly defined for shocks with chemistry, and we have chosen the special definition given in § V.

non–LTE excitation, and rate of cooling by H_2 molecules were calculated in detail, using collision rate constants and other atomic data as in Draine and Katz (1986*a*). For the adopted initial conditions, we find that shocks are C-type if $v_s \lesssim 5$ km s^{-1}, J-type if $5 \lesssim v_s \lesssim 18$ km s^{-1}, and type C* if $18 \lesssim v_s \lesssim 30$ km s^{-1}. For this set of preshock conditions, the peak temperature of the neutral gas was found to increase monotonically with v_s, to a value $T_{n,\max} = 1.1 \times 10^4$ K in the 30 km s^{-1} model. Because our computer codes do not include some physical processes relevant at temperatures much higher than 10^4 K, we have not yet simulated shocks with $v_s > 30$ km s^{-1}. However, we note that dissociation of H_2 in the 30 km s^{-1} model was moderate—$n(H_2)/n_H$ declined to 0.029 from its initial (preshock) value of 0.035—so that we cannot exclude the possibility that C* shocks will be found at somewhat higher shock speeds.

Figure 9 is the hydrodynamical profile of a J shock with $v_s = 10$ km s^{-1} which, for the preshock conditions in Table 1, corresponds to $M_{nA} = 5.4$. The total energy and momentum fluxes are conserved to within errors of about 1% in this model. Notice

that the compression ratio across the jump front in Figure 9*a* is only 1.6; in fact, this is the *largest* compression ratio found in the exemplary sequence of models. The peak neutral temperature in Figure 9*b* is about 2100 K, 0.91 times the maximum temperature that would be found in a single-fluid shock or in an adiabatic shock with the same parameters.

Figure 9*c* is the phase portrait of this model, as computed from our numerical solution. Because our models include chemistry, the fluid variables T_n, T_i, and T_e, as well as the chemical abundances n_j/n_H, are not defined unambiguously at points that lie off the solution trajectory. Consequently, we adopt the following prescription for finding points (q, r) on the $R = 0$ curve: For each v_n and v_i on the computed solution trajectory, we take $q = v_i/v_s$ and find, numerically, the value of $r = v_n/v_s$ for which the numerator in equation (1) vanishes. In computing the value of the numerator, we (a) hold T_i, T_e and the chemical abundances fixed at their values on the solution curve at the same q-value, and (*b*) find T_n from the requirement that the total momentum flux should be conserved everywhere in the phase plane. We find the locus of points where $M = 1$ by an analogous procedure. While this procedure is *ad hoc* in nature, it correctly locates intersections of the solution with $M = 1$ and $R = 0$. To the extent that the chemistry and fluid dynamics are weakly coupled in the models considered here, the phase portrait is insensitive to this procedure.

Figure 10 shows analogous results for a C* shock, with $v_s = 20$ km s^{-1} and $M_{nA} = 10.8$. The maximum departures from energy and momentum conservation in this numerical solution were about 1%. Despite the small abundance of molecular hydrogen, about 3% in this model, the absence of adiabatic compression and heating at a jump front allows the neutral gas to stay relatively cool: the peak neutral temperature in Figure 10*b* is 6500 K, about 0.59 times the value to be found in a single-fluid shock with the same parameters.

VI. DISCUSSION

It was demonstrated above that, under certain conditions, the sonic points in MHD shocks attract the trajectories in an infinitesimal neighborhood of phase space. While this fact makes it plausible that C* solutions should be realized for *some* sets of shock parameters, it cannot explain why C* solutions occupy a large fraction of parameter space, both in our realistic simulations and in the analytical simulations summarized in Figure 7*b*. There is evidently some *global* attraction mechanism at work in such cases, which forces the solution trajectory into the upstream sonic point's local domain of attraction. The examples given here and in Chernoff's paper (C87) suggest that the hypothetical mechanism operates when (a) M_{nA} is large and (b) the neutral cooling rate is a rapidly increasing function of T_n.

To see why these circumstances favor C* shocks, consider the evolution of a fluid element as it passes through the initial, supersonic part of the flow. Chernoff (C87) showed that if M_{nA} is large, then compression of the charged fluid takes place on a length scale L_i that is much shorter than the scale L_n on which the neutrals are compressed. In this case, the momentum equations for the charged and neutral fluids are approximately

$$\frac{d}{dz}\left(\frac{v_s^2}{v_i^2}\frac{B_0^2}{8\pi}\right) = -F_n\,, \tag{6.1}$$

and

$$\frac{d}{dz}(\rho_n v_n^2) = F_n\,, \tag{6.2}$$

respectively. In equation (6.1), the assumption of low fractional ionization has been used to neglect thermal and ram pressure of the charged particles in comparison to $B^2/8\pi$. In equation (6.2), neutral thermal pressure has been neglected in comparison to ram pressure, because we are interested in the initial part of the solution, where the neutral Mach number is large. Dimensional analysis of equations (6.1) and (6.2) implies that, initially, $L_i/L_n \sim M_{nA}^{-2}$ (C87). Thus, although the forces on the ions and neutrals are identical in magnitude, the ions are compressed more rapidly because, when M_{nA} is large, the momentum flux $\rho_{n0} v_s^2$ initially present in the neutrals is large compared to the momentum flux $B_0^2/8\pi$ in the ion-electron fluid. Shock solutions for large M_{nA} must therefore begin by moving horizontally to the left in the phase plane. Thereafter, the phase trajectory must move almost vertically downward inside the "thermal envelope" of allowed temperatures. Since the neutrals are heated (by ion-neutral scattering) as they are decelerated, compression of the neutrals is accompanied by an abrupt rise in temperature and a corresponding drop in the neutral Mach number. The trajectory, therefore, moves downward toward the $M = 1$ curve which, when M_{nA} is large, lies well above the $q = r$ line (compare Figs. 8*a* and 8*d*).

Now consider the various forces on a fluid element as $M \to 1$. According to equation (3.1), the neutrals in a steady flow experience an acceleration given, in dimensionless units, by

$$r\frac{dr}{dz'} = r\left[\frac{q-r}{r} - \frac{d}{dz'}\left(\frac{t}{r}\right)\right]. \tag{6.3}$$

The first term in brackets is just the dimensionless expression for F_n, the drag force per unit volume due to elastic ion-neutral scattering. The preceding discussion shows that $q - r < 0$, so ion-neutral drag always decelerates the neutrals. The second term in brackets is the dimensionless gradient of the neutral thermal pressure, t/r; pressure forces alone can either accelerate or decelerate the neutrals, depending on the values of $\dot{r}$ and $\dot{t}$. The quantity $\dot{r}$ is negative everywhere in the compressive waves considered in this paper, so that pressure gradients and drag forces act in the same direction whenever the neutral temperature is rising. However, if $\dot{t} \ll 0$, i.e., if neutral cooling is sufficiently rapid, then the pressure gradient opposes drag. In the latter case, it becomes possible for the acceleration of the neutrals, and thus their rate of compression, to vanish. The locus of points in phase space where this occurs is just the $R = 0$ line.

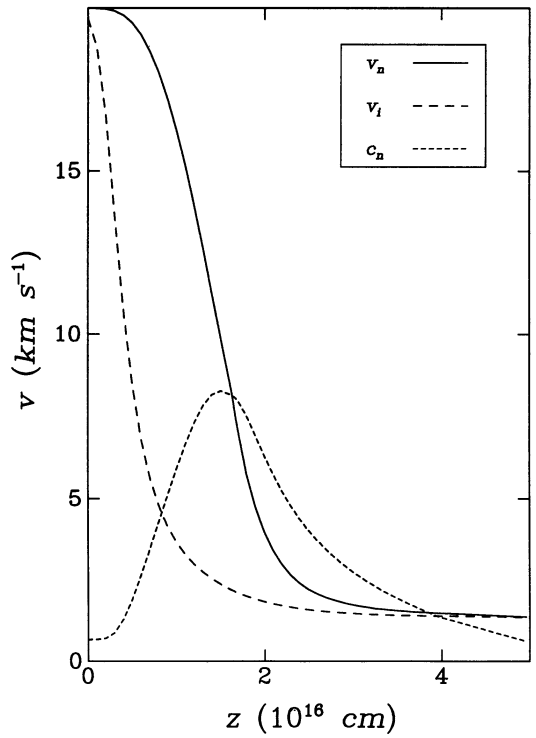

FIG. 10*a*

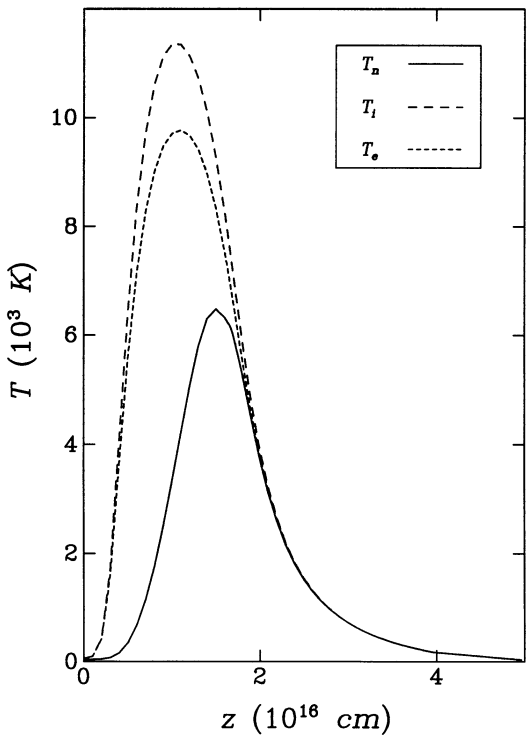

FIG. 10*b*

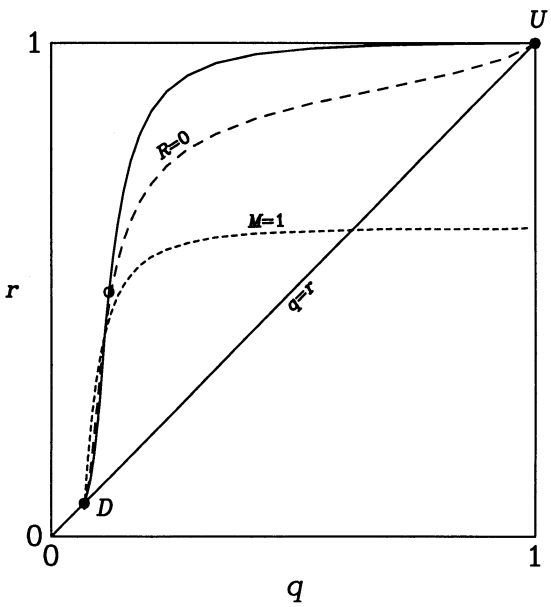

FIG. 10*c*

FIG. 10.—Same as Fig. 9, but for a C* shock. Initial conditions are identical to those for Fig. 9, except that the shock speed is 20 km s^{-1}. Maximum temperature attained by the neutrals is $T_{n,\max} = 6474$ K, which is 0.59 of the peak temperature which would have been attained in a single fluid shock, or in the absence of cooling.

It is now possible to see why details of the neutral cooling determine the shock type. Consider, once again, a fluid element on the rapidly descending portion of the phase trajectory, at the point where M has dropped to unity. If neutral cooling is absent or is sufficiently weak, then $R \neq 0$ at the point in question; i.e., the $R = 0$ curve must lie below $M = 1$ (see Figs. 8*b* and 9*c*). This case corresponds to a J shock. Consider next an alternative possibility, in which an efficient cooling mechanism "switches on" as T_n rises above some threshold value. As the neutral cooling rate increases, the $R = 0$ curve moves above $q = r$, because when $\dot{t} \ll 0$, a large drag force is required to balance the pressure gradient in equation (6.3). If the switched-on cooling is sufficiently rapid, then $R = 0$ can move above $M = 1$ (Figs. 8*c*, 10*c*). In this case, the topology of $R = 0$ and $M = 1$ makes it impossible for the trajectory to become subsonic without crossing $R = 0$. In fact, the trajectory can never reach $R = 0$, where $\dot{r} = 0$, because compression of the *charged* fluid by drag forces, which can never vanish, makes the trajectory drift to the left and away from $R = 0$. However, since the length scale for ion compression greatly exceeds the scale for neutral compression in this part of the flow, the neutrals always remain

close to $R = 0$. To put it succinctly, strong neutral cooling forces the neutrals to remain close to states (on $R = 0$) where the neutral acceleration vanishes. Compression of the ions by drag forces, which can never cease, gradually shifts those states toward smaller q values; the trajectory is funneled along $R = 0$ and into the sonic point. (Note that, for points downstream from the neutral temperature peak in Fig. 10*c*, the neutral compression ratio never differs by more than a few percent from the value for which $R = 0$.)

The funneling by $R = 0$ of trajectories into the sonic point is the global attraction mechanism hypothesized above. The operation of this mechanism depends on the topology of $R = 0$ and $M = 1$ in phase space which, according to the discussion in § III*d*, is sensitive to details in the cooling function. However, our numerical simulations (Figs. 9 and 10) show that diffuse cloud shocks display this behavior, i.e., are C* shocks, at intermediate shock speeds $18 \lesssim v_s \lesssim 30$ km s^{-1}. We attribute this result to the switching on of H_2 rotation-vibration cooling at temperatures of a few thousand Kelvins. Finally, it should be noted that analogous phenomena have been discovered in other gasdynamic problems. In the case of spherical stellar winds, for example, smooth transonic flows are found to become possible when heat and momentum transfer processes are introduced into the equations of motion for an adiabatic wind (see Holzer and Axford 1970). Indeed, Figures 3*a*–3*c* have exact counterparts in such flows (although the phase variables and critical lines have different meanings; see Holzer 1977, Fig. 2).

VII. SUMMARY

The main conclusions of this paper are as follows.

1. We have found a new class of solutions, called C* shocks, to the equations of motion for multifluid, MHD shock waves.
2. The existence of C* shocks is possible because sonic points can act as attractors, both locally and globally, in the phase of shock solutions. The attractorlike properties of sonic points are determined by the cooling properties of shock-heated plasmas.
3. We have developed numerical methods for simulating J-type and C* shocks propagating in diffuse interstellar clouds.
4. In a limited set of numerical models, calculated for illustrative purposes, C* solutions were found for a variety of realistic shock parameters. The peak neutral temperature attained in a C* shock may be appreciably lower than in a single-fluid shock, so that chemistry and line emission are both sensitive to the shock structure.

The authors wish to acknowledge helpful discussions with Mary Brewster and Julian Cole. We are particularly indebted to Mark Wardle for pointing out that the special transonic trajectories can be found analytically and to Telemachos Mouschovias for pointing out the analogy with stellar winds. This work was partially supported by a grant from NASA, administered by the American Astronomical Society, by a Dudley Observatory Career Development Award to W. G. R., and by grants AST-8341412 and AST-8612013 from the National Science Foundation.

APPENDIX A

ARTIFICIAL VISCOSITY METHODS FOR COMPUTING J SHOCKS

In a recent paper (FPdF87), Flower and Pineau des Forêts presented a method for computing J-type shocks, using an implicit form of artificial viscosity. Their scheme replaces equation (2.1) with the expression

$$\frac{dv_n}{dz} = \frac{2/3[G_n - N_n u_n - (\rho_n v_n/\mu_n)(du_n/dz)] - F_n v_n + S_n v_n^2}{-\rho_n(|c_n^2 - v_n^2| + \delta)}, \tag{A1}$$

where δ is a positive constant and integrates the entire flow using an initial value method. Since the denominator of equation (A1) never vanishes, the numerical difficulties encountered with integrations of equation (2.1) near sonic points are avoided. The nominal justification for this procedure is that equation (A1) is an excellent approximation for $|dv_n/dz|$ whenever $|M^2 - 1| \gg \delta/c_n^2$. Choosing $\delta = 10^7$ cm^2 s^{-2} as in FPdF87 and taking $c_n = 5$ km s^{-1} as a typical value for the sound speed in shock-heated gas, we see that the approximation is good whenever $|M - 1| \gg 10^{-3}$, i.e., except for regions of phase space very close to sonic points. Notice, however, that the denominator on the right-hand side of equation (A1) fails to change sign as a trajectory crosses the $M = 1$ curve, as the correct equation of motion (2.1) demands.

Unfortunately, the method of FPdF87 is invalid for several reasons, as the following example demonstrates. Consider the calculation of an adiabatic shock wave ($H_n \equiv 0$), propagating in a gas where the fractional ionization is low, so that equation (3.8) is an excellent description of the hydrodynamics. When $H_n \equiv 0$, equation (3.8) reduces to

$$\frac{dr}{dq} = \frac{(\gamma - 1)r[\gamma r/(\gamma - 1)r - q]}{M_{nA}^2 q^3(\gamma t - r^2)}. \tag{A2}$$

If one follows the steps in C87 leading to equation (A2), but with equation (2.1) replaced with equation (A1), the result is

$$\frac{dr}{dq} = \frac{-(\gamma - 1)r[\gamma r/(\gamma - 1)r - q]}{M_{nA}^2 q^3[|(\gamma t - r^2)| + \delta_*]}, \tag{A3}$$

where $\delta_* \equiv \delta/v_s^2$. In other words, the prescription of FPdF87 reduces to equation (A3) under conditions for which equation (A2) exactly describes the hydrodynamics.

In Figure 11, we compare the solution of equation (A3), obtained by numerical integration, with the exact solution of equation (A2), as given in C87. Both solutions were computed for $\gamma = 5/3$ and $M_{nA} = 10$, which guarantees that the exact solution is a J shock

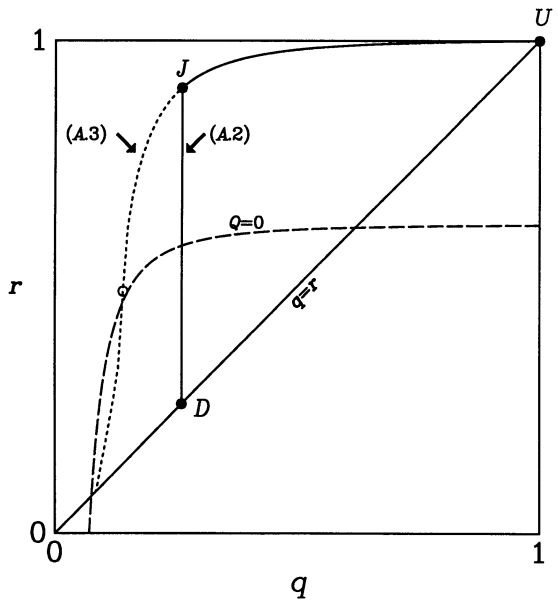

FIG. 11.—Phase portrait of an adiabatic MHD shock with neutral Alfvén Mach number $M_{nA} = 10$. Curve labeled "A.2" is the exact solution of eq. (A2) as given by C87, which accurately describes the hydrodynamics at sufficiently low fractional ionization. Curve labeled "A.3" is a numerical solution of eq. (A3), which describes the method proposed by Flower and Pineau des Forêts (1987) for calculating J-type shocks. Open circle indicates the point of maximum T_n on the solution to eq. (A3). The exact solution attains a maximum in T_n at point D.

(C87). The parameter δ_* was chosen small enough to make the numerical solution independent of δ_* at the 1% level. As predicted by FPdF87, equations (A3) and (A2) give nearly identical results upstream from point J, where the jump occurs. However, equation (A3) gives a very poor approximation to the exact solution elsewhere. For example, it overestimates the compression at the downstream equilibrium point, by roughly a factor of 3: The exact solution jumps directly to the final state $q = r = 0.26$, but the solution of equation (A3) terminates at $q = r = 0.084$. Equation (A3) also fails to conserve energy; the discrepancy between the initial and final total energy fluxes is about 300% in the FPdF87 solution.

In their paper, Flower and Pineau des Forêts give a numerical solution, obtained with their method, that agrees well with a shock calculated in D80 for similar parameter values. The agreement, which the preceding discussion shows to be fortuitous, can be explained as follows. For parameters corresponding to a J shock, the method of FPdF87 yields a phase space solution trajectory that crosses $M = 1$ to the left of the correct position of the jump, because their method assumes implicitly that the jump occurs where M is close to unity (see Fig. 5). Once it crosses $M = 1$, the trajectory moves downward in the "forbidden region" between $M = 1$ and $R = 0$, where trajectories that obey the correct equations should move *upward*. Because it cannot cross $R = 0$, the hypothetical FPdF87 solution must eventually flow onto, and then along, the $R = 0$ curve, it is actually excluded from the subsonic region where the true solution must lie. Notice, however, that there is also a tendency for an exact J-type solution to follow the $R = 0$ curve, *but on the opposite side* (see Fig. 9*c*). This is the source of the agreement cited by FPdF87. Such agreement cannot be anticipated in general.

There are several reasons why the method of FPdF87 is invalid. First and most important, it is incorrect to assume that the solution is insensitive to small errors near the sonic point. The nozzle-like behavior of the phase flow near C (Fig. 3) implies that an infinitesimal error in the solution near C can result in large errors downstream. This is related to a second problem with the FPdF87 method: it takes no account of the boundary-value aspect of the subsonic flow. The method proposed here also makes errors in the flow near sonic points, but the shooting method uses one's knowledge of the downstream boundary conditions to limit the downstream propagation of such errors. A third problem with the FPdF87 method is that artificial dissipation is inserted very close to the sonic point implying, incorrectly, that the exact solution is a very weak shock. Fourth, the FPdF87 method always gives a solution in which the sign of dv_n/dz is incorrect, throughout some region of the flow. And finally, *ad hoc* prescriptions of this type for the artificial viscosity will generally fail to conserve momentum and energy; as shown in the example above, the error can be large. A correct implementation of artificial viscosity must include the "artificial" stress tensor in both the energy equation and the momentum equation, because dissipation is inevitably associated with any "viscous stress."

APPENDIX B

PHASE FLOW NEAR SONIC POINTS

The phase flow near a sonic point consists of the trajectories $r(q)$ that satisfy equation (3.14) and is determined completely by the three parameters α, ϕ, and η. Here it is shown that just four generic flow families exist. The analysis is simplest if one transforms the "velocity vector" $(\dot{q}, \dot{r})$ to polar coordinates, giving

$$\rho\dot{\theta} = \dot{q}_c\left[\alpha \cos\theta \frac{\sin(\theta - \phi)}{\sin(\theta - \eta)} - \sin\theta\right], \tag{B1a}$$

and

$$\dot{\rho} = \dot{q}_c\left[\alpha \sin\theta \frac{\sin(\theta-\phi)}{\sin(\theta-\eta)} + \cos\theta\right] \tag{B1b}$$

The constant $\dot{q}_c$, which is negative in the phase space regions of physical interest, is the derivative of q in equation (3.6), evaluated at (q_c, r_c). The trajectories of equation (B1) depend on ratios of the above derivatives and are therefore independent of $\dot{q}_c$. It follows from equation (B1) that there are no fixed points when $\dot{q}_c \neq 0$, because $\dot{\rho}(\theta) = \dot{\theta}(\theta) = 0$ would imply $\tan^2(\theta) = -1$. It is also evident that the flow is symmetric, with $\dot{\rho}(\theta+\pi) = -\dot{\rho}(\theta)$ and $\rho\dot{\theta}(\theta+\pi) = -\rho\dot{\theta}(\theta)$.

I. SPECIAL TRANSONIC TRAJECTORIES

Suppose that $\dot{\theta}$ vanishes for some $\theta = \hat{\theta}$. Then, since equation (B1) has no fixed points, and $\rho\dot{\theta}$ depends only on θ, one of the solutions of equations (B1) is a straight line passing through the sonic point with $\theta = \hat{\theta}$. The zeros of $\dot{\theta}$ can be found explicitly in terms of α, η, and ϕ. Multiplication of $\rho\dot{\theta}/\dot{q}_c = 0$ by $\sin(\hat{\theta}-\eta)/\cos^2(\hat{\theta})$ yields a quadratic in $\tan\hat{\theta}$ with roots

$$\tan\hat{\theta}_{1,2} = \frac{\sin\eta + \alpha\cos\phi \mp W^{1/2}}{2\cos\eta}, \tag{B2a}$$

$$W \equiv \alpha^2\cos^2\phi + 2\alpha(\sin\eta\cos\phi - 2\sin\phi\cos\eta) + \sin^2\eta\,. \tag{B2b}$$

Real solutions (eq. [B2]) exist only for values of α such that $W \geq 0$. Suppose $W = 0$ for $\alpha = \alpha_{\rm crit}$. Then $\alpha_{\rm crit}$ must satisfy

$$A\alpha_{\rm crit}^2 + B\alpha_{\rm crit} + C = 0\,, \tag{B3a}$$

$$A \equiv \cos^2\phi\,, \tag{B3b}$$

$$B \equiv 2(\sin\eta\cos\phi - 2\sin\phi\cos\eta)\,, \tag{B3c}$$

$$C \equiv \sin^2\eta\,. \tag{B3d}$$

Real solutions for $\alpha_{\rm crit}$ exist if and only if the quantity

$$B^2 - 4AC = 16\sin\phi\cos\eta\sin(\phi-\eta) \tag{B4}$$

is positive.

The trajectories $\hat{\theta}_1$ and $\hat{\theta}_2$ have the following special property. Consider the phase flow upstream from a sonic point, in the neighborhood of $\hat{\theta}_k$ (where $k = 1$ or 2). Suppose that as θ increases through $\hat{\theta}_k$, the derivative $\dot{\theta}$ goes through zero by passing from positive to negative values. Then all trajectories within some range of θ values near $\hat{\theta}_k$ will have $(d/dz)|\theta - \hat{\theta}_k| < 0$, i.e., they will be *attracted* to $\hat{\theta}_k$. Further, since the phase velocity dr/dq is unique outside the sonic point, all trajectories in the domain of attraction must pass along with $\hat{\theta}_k$ into the subsonic region. It is easily seen that the domain of attraction is a cone, delimited on either side of $\hat{\theta}_k$ by those lines (including possibly $M = 1$) where $\dot{\theta}$ undergoes another sign change. A similar argument shows that, in the other possible case where $\dot{\theta}$ passes from negative to positive values at $\hat{\theta}_k$, the special trajectory $\hat{\theta}_k$ *repels* trajectories in a finite domain. Notice that the symmetry of the phase flow guarantees that the attractive/repulsive character of a special trajectory must reverse on the downstream side of a sonic point.

II. THE UPSTREAM SONIC POINT $(0 < \eta < \phi < \pi/2)$

Since $\phi > \eta$, $B^2 - 4AC > 0$, and $\alpha_{\rm crit}$ is given by

$$\alpha_{\rm crit}^{\pm} = \frac{\sin\phi\cos\eta + \sin(\phi-\eta) \pm 2[\sin\phi\cos\eta\sin(\phi-\eta)]^{1/2}}{\cos^2\phi}\,. \tag{B5}$$

Thus, $W > 0$ for $\alpha < \alpha_{\rm crit}^-$ or $\alpha > \alpha_{\rm crit}^+$ and there are two disjoint families of solutions for $\hat{\theta}$ depending on the value of α. The physically meaningful solutions can be inferred from a graph of $\rho\dot{\theta}$ versus θ, if one notes the limits of $\dot{\theta}$ as $\theta \to 0, \eta^+, \eta^-$, and $\pi/2^-$, plus the fact that there are at most two solutions.

The result of such an analysis is that there are three possibilities for the flow: if $\alpha \leq \alpha_{\rm crit}^-$, then the two roots for $\hat{\theta}$ satisfy $0 \leq \hat{\theta}_1 \leq \hat{\theta}_2 < \eta$. This case is shown in Figure 3*a*; upstream from the sonic point, $\hat{\theta}_1$ repels trajectories and $\hat{\theta}_2$ attracts them. The domain of attraction of $\hat{\theta}_2$ includes trajectories in the subsonic phase space cone between $\hat{\theta}_1$ and $M = 1$, all of which are funneled into the supersonic region via the sonic point. The downstream reversal of attraction and repulsion disperses the flow as it emerges from the sonic point. The next generic case, shown in Figure 3*b*, occurs when $\alpha_{\rm crit}^- < \alpha < \alpha_{\rm crit}^+$ so that there are no roots for $\hat{\theta}$. The phase flow then consists entirely of trajectories that are emitted and/or absorbed by the $M = 1$ line. The final possibility, $\alpha_{\rm crit}^+ \geq \alpha$, has two roots with $\phi < \hat{\theta}_1 \leq \hat{\theta}_2 < \pi/2$. Trajectory $\hat{\theta}_1$ is an attractor and $\hat{\theta}_2$ is a repellor. In contrast to the first case above, however, *supersonic* trajectories are funneled into the *subsonic* region. One concludes that a continuous transition from supersonic to subsonic flow may exist only if

$$\alpha > \alpha_{\rm crit}^+ \equiv \frac{\sin\phi\cos\eta + \sin(\phi-\eta) + 2[\sin\phi\cos\eta\sin(\phi-\eta)]^{1/2}}{\cos^2\phi}\,, \tag{B6}$$

at the upstream sonic point.

III. THE DOWNSTREAM SONIC POINT ($0 < \phi < \eta < \pi/2$)

Equation (B5) shows that $B^2 - 4AC < 0$ and there are no α values for which $W = 0$. Since W is a continuous function of α, and $W(\alpha = 0) = \sin^2 \eta > 0$, it follows that $W > 0$ for all α. Thus there are always two special trajectories at the downstream sonic point. A graphical analysis analogous to the one outlined above shows that the two roots satisfy $0 < \hat{\theta}_1 < \phi$ and $\eta < \hat{\theta}_2 < \pi/2$. For the phase space topology assumed here (two sonic points), the solution trajectory must emerge from the sonic point C′ on $\hat{\theta}_1$, where

$$\tan \hat{\theta}_1 = \frac{\sin \eta + \alpha \cos \phi - W^{1/2}}{2 \cos \eta} . \tag{B7}$$

The phase flow is a saddle point.

APPENDIX C

ADIABATIC SHOCK CONDITIONS

We seek to determine the compression ratio and peak temperature achieved in a fully adiabatic MHD shock. We use the dimensionless variables of equation (3.1)–(3.3) and allow for an arbitrary preshock temperature $t_0 \equiv kT_{n0}/\mu_n v_s^2$. Equation (3.5), obtained from combining the two equations of momentum conservation (eqs. [3.1] and [3.2]), generalizes to

$$t(q, r) = r[1 + t_0 - r + \tfrac{1}{2} M_{nA}^{-2}(1 - q^{-2})] . \tag{C1}$$

Now multiply equation (3.2) by q and add to equation (3.3) to obtain the overall equation of energy conservation:

$$\frac{d}{dz'}\left[M_{nA}^{-2} q^{-1} + \frac{1}{2} r^{-2} + \frac{\gamma}{(\gamma - 1)} t \right] = H_n = 0 . \tag{C2}$$

To find the downstream state $q_{ad} = r_{ad}$ reached in an adiabatic shock, we set $q = r$, substitute equation (C1) into equation (C2), and multiply by $2(\gamma - 1)r$ to obtain the cubic equation

$$(\gamma + 1)r^3 - 2\gamma(1 + t_0 + \tfrac{1}{2} M_{nA}^{-2})r^2 + [(\gamma - 1)(1 + 2M_{nA}^{-2}) + 2\gamma t_0]r + M_{nA}^{-2}(2 - \gamma) = 0 . \tag{C3}$$

Factor out the trivial root $(r - 1)$ to obtain the quadratic

$$(\gamma + 1)r^2 - [\gamma - 1 + \gamma(2t_0 + M_{nA}^{-2})]r - (2 - \gamma)M_{nA}^{-2} = 0 , \tag{C4}$$

a result obtained previously by Field *et al.* (1968). Equation (C4) has the positive root

$$r_{ad} = \frac{(\gamma - 1) + \gamma(2t_0 + M_{nA}^{-2}) + \{[(\gamma - 1) + \gamma(2t_0 + M_{nA}^{-2})]^2 + 4(\gamma + 1)(2 - \gamma)M_{nA}^{-2}\}^{1/2}}{2(\gamma + 1)} . \tag{C5}$$

For compression to take place ($r_{ad} < 1$), it is necessary that $M_{nA}^2 > (1 - \gamma t_0)^{-1}$, which is equivalent to $v_s > (\gamma kT_{n0}/\mu_n + B_0^2/4\pi\rho_{n0})^{1/2}$: the shock speed must exceed the magnetosonic speed.

REFERENCES

Bender, C. M., and Orszag, S. A. 1978, *Advanced Mathematical Methods for Scientists and Engineers* (New York: McGraw-Hill).
Chernoff, D. F. 1987, *Ap. J.*, **312**, 143 (C87).
Chernoff, D. F., Hollenbach, D. J., and McKee, C. F. 1982, *Ap. J. (Letters)*, **259**, L97.
Draine, B. T. 1978, *Ap. J. Suppl.*, **36**, 595.
———. 1980, *Ap. J.*, **241**, 1021 (D80).
———. 1986*a*, *M.N.R.A.S.*, **220**, 133.
———. 1986*b*, *Ap. J.*, **310**, 408.
Draine, B. T., and Katz, N. S. 1986*a*, *Ap. J.*, **306**, 655.
———. 1986*b*, *Ap. J.*, **310**, 392.
Draine, B. T., and Roberge, W. G. 1982, *Ap. J. (Letters)*, **259**, L91.
Draine, B. T., and Salpeter, E. E. 1979, *Ap. J.*, **231**, 438.
Field, G. B., Rather, J. D. G., Aannestad, P. A., and Orszag, S. A. 1968, *Ap. J.*, **151**, 953.
Flower, D. R., and Pineau des Forêts, G. 1987, *M.N.R.A.S.*, **224**, 403 (FPdF87).
Gear, C. W. 1971, *Numerical Initial Value Problems in Ordinary Differential Equations* (Englewood Cliffs: Prentice Hall).
Hollenbach, D. J., Chernoff, D. F., and McKee, C. F. 1989, in *22nd ESLAB Symposium, Infrared Spectroscopy in Astronomy*, in press.
Hollenbach, D. J., and McKee, C. F. 1979, *Ap. J. Suppl.*, **41**, 555.
Holzer, T. E. 1977, *J. Geophys. Res.*, **82**, 23.
Holzer, T. E., and Axford, W. I. 1970, *Ann. Rev. Astr. Ap.*, **8**, 31.
Landau, L. D., and Lifshitz, E. M. 1959, *Fluid Mechanics* (New York: Pergamon).
McCray, R., and Snow, T. P. 1979, *Ann. Rev. Astr. Ap.*, **17**, 213.
Mullan, D. J. 1971, *M.N.R.A.S.*, **153**, 145.
Pineau des Forêts, G., Flower, D. R., Hartquist, T. W., and Dalgarno, A. 1986, *M.N.R.A.S.*, **220**, 801.
Press, W. H., Flannery, B. P., Teukolsky, S. A., and Vetterling, W. T. 1986, *Numerical Recipes* (New York: Cambridge University Press).
Shull, J. M., and McKee, C. F. 1979, *Ap. J.*, **227**, 131.
Troland, T. H., and Heiles, C. 1986, *Ap. J.*, **301**, 339.
Wardle, M. 1990, in preparation.
Wardle, M., and Draine, B. T. 1987, *Ap. J.*, **321**, 321.

B. T. DRAINE: Peyton Hall, Princeton University, Princeton, NJ 08544-1001

W. G. ROBERGE: Department of Physics, Rensselaer Polytechnic Institute, Troy, NY 12180-3590